RHEOLOGICAL EFFECTS ON ULTRA-FINE GRINDING IN STIRRED MILLS

by

JIAN YUE

B. Eng. Xian University of Science and Technology, China, 1983

A THESIS SUBMITTED IN PARTIAL FULFILMENT OF
THE REQUIREMENTS FOR THE DEGREE OF

Master of Applied Science

in

THE FACULTY OF GRADUATE STUDIES

(Department of Mining Engineering; the University of British Columbia)

We accept this thesis as conforming
to the required standard

THE UNIVERSITY OF BRITISH COLUMBIA

August 2003

In presenting this thesis in partial fulfilment of the requirements for an advanced degree at the University of British Columbia, I agree that the Library shall make it freely available for reference and study. I further agree that permission for extensive copying of this thesis for scholarly purposes may be granted by the head of my department or by his or her representatives. It is understood that copying or publication of this thesis for financial gain shall not be allowed without my written permission.

Department of Mining Engineering

The University of British Columbia
Vancouver, Canada

Date Sep 15, 2003

DE-6 (2/88)

Summary

A pilot scale study was conducted on ultra-fine grinding in a horizontal stirred mill. The main objectives were to investigate grinding kinetics, the influences of rheology and effects of bead size on performance criteria. The main criteria were breakage rate, particle size reduction, product size distribution and power consumption.

The results confirm the "first-order" breakage rates in stirred mills. The product size distributions are best represented by the Rosin-Rammler equation. A method of determining breakage rates versus particle size is demonstrated which shows that the 10% top size fraction is most appropriate for the determination of specific breakage rates.

The slurries ground exhibit Newtonian to pseudoplastic to yield pseudoplastic behavior over the range of conditions studied, corresponding to coarse low percentage solids to fine high percentage solids. The flow curves of grinding products were modeled using the Casson equation. It was shown that yield stress is the dominant rheological parameter which influences the grinding performance. A Low yield stress favors high breakage rates, narrow size distributions, and increased production of -10 μm fines.

The bead sizes and its composition play a very important role in stirred mills. There exists an optimum ratio of bead size to feed size with respect to breakage rate, size reduction ratio and size distribution. The ratio was confirmed to be about 20/1. The existence of fine beads in grinding media has negative effects on grinding performance.

TABLE OF CONTENTS

Summary.....ii

Table of Contents.....iii

List of Figures.....v

List of Tables.....viii

List of Symbols.....ix

Acknowledgements.....xi

CHAPTER 1 Introduction.....1

1.1 Background.....1
1.2 Objectives.....5
1.3 Methodology.....6

CHAPTER 2 Experimental Program.....8

2.1 Introduction.....8
2.2 Experimental System
2.2.1 Equipment and Instruments.....8
2.2.2 Grinding Material.....10
2.3 Test Design and Procedures.....11
2.3.1 Sampling.....11
2.3.2 Breakage Kinetic Tests.....11
2.3.3 Rheology Tests.....13
2.3.4 Bead Size Tests.....13

CHAPTER 3 Particle Breakage Kinetics in Horizontal Stirred Mills.....14

3.1 Introduction.....14
3.2 Literature Review.....14
3.3 Procedures.....16
3.4 Results and Discussions.....16
3.4.1 Product Size Distribution.....16
3.4.2 Breakage Rate.....22
3.4.3 Breakage Rate versus Particle Size.....24
3.4.4 Grinding Limit.....26
3.4.5 Breakage Mechanisms.....28

3.5 Conclusions....29
3.6 Recommendations....30

CHAPTER 4 Rheological Effects on Ultra-Fine Grinding in Stirred Mills....31

4.1 Introduction....31
4.2 Literature Review....31
4.3 Procedures....35
4.4 Results and Discussions....35
4.4.1 Flow-Curve Modeling....35
4.4.2 Effect of Solid Content and Particle Size....38
4.4.3 Breakage Rate....42
4.4.4 Fines Production....45
4.4.5 Particle Size Distribution....46
4.4.6 Power....47
4.5 Conclusions....49
4.6 Recommendations....51

CHAPTER 5 Effects of Bead Size on Ultra-Fine Grinding in Stirred Mills....52

5.1 Introduction....52
5.2 Literature Review....52
5.3 Experiments....55
5.4 Results and Discussions....55
5.4.1 Mono-sized grinding beads....55
5.4.2 Bead Size Distribution....62
5.5 Conclusions....67
5.6 Recommendations....68

CHAPTER 6 Conclusions and Recommendations....69

6.1 Conclusions....69
6.2 Recommendations....71

References....73

Appendix A Grinding Kinetics and Rheology....77

Appendix B Bead Size Testing....86

List of Figures

Figure 2.1 The experimental system for ultra-fine grinding tests

Figure 2.2 Schematic diagram of elongated fixture for rheological measurement of settling suspensions

Figure 2.3 Feed size distributions

Figure 2.4 Equilibrium test for sampling in the stirred bead mill

Figure 3.1 Correlation coefficient of both fitted models vs. test number

Figure 3.2 Relationship between distribution modulus and correlation coefficient

Figure 3.3 Relationship between particle size and correlation coefficient

Figure 3.4 Rosin-Rammler particle size distribution modulus versus product size P_{80}

Figure 3.5 Particle size distribution of feed sample with fitted Rosin Rammler equation

Figure 3.6 Particle size distribution products from five cycles of grinding with fitted Rosin-Rammler equation

Figure 3.7 Breakage rate versus resident time for the +97 μm fraction

Figure 3.8 Breakage rate versus resident time for the +64 μm fraction

Figure 3.9 Specific breakage rate vs. top particle size fractions representing 5, 10 and 20 percentiles

Figure 3.10 Specific breakage rate vs. top particle size fraction

Figure 3.11 Particle size reduction ratio versus feed size F_{80}

Figure 3.12 Size distribution for stirred mill products following successive grinds

Figure 4.1 Common rheological flow-curves

Figure 4.2 Flow-curves of fine quartz suspension (Casson Fitted, 40% Solids)

Figure 4.3 Flow-curves of quartz suspension with Bingham fitting (40% solids)

Figure 4.4 Yield stress vs. solid content of slurries tested

Figure 4.5 Yield Stress vs. Particle size

Figure 4.6 Casson viscosity vs. solid content

Figure 4.7 Casson viscosity vs. particle size P_{80}

Figure 4.8 Apparent viscosity ($50\ s^{-1}$) vs. particle size P_{80}

Figure 4.9 Apparent viscosity ($300\ s^{-1}$) vs. particle size P_{80}

Figure 4.10 Specific breakage rate vs. pulp density with different top size fractions

Figure 4.11 Specific breakage rate vs. pulp yield stress

Figure 4.12 Specific breakage rate vs. particle sizes

Figure 4.13 Net production of -10 μm production rates vs. yield stress of slurries

Figure 4.14 Rosin-Rammler particle size distribution coefficient vs. slurry yield stress

Figure 4.15 Agitator power vs. yield stress of slurries tested

Figure 4.16 Agitator power vs. Casson viscosity of slurries tested

Figure 5.1 Specific breakage rate vs. bead size

Figure 5.2 P_{80} vs. grinding bead size

Figure 5.3 Particle size distribution modulus vs. bead sizes

Figure 5.4 Agitator power vs. bead sizes

Figure 5.5 Schematic diagram of beads and particles in a stirred mill

Figure 5.6 Schematic diagram of impact and compression breakage mechanism

Figure 5.7 Bead bulk density vs. fine fraction of bi-modal beads

Figure 5.8 Specific breakage rate vs. % fine bead

Figure 5.9 Product size P_{80} vs. grinding bead size

Figure 5.10 Particle distribution modulus vs. % fine bead

Figure 5.11 Agitator power vs. % fine bead

Figure A.2.1 Particle size distributions for test series 3 (35% solids)

Figure A.2.2 Particle size distributions for test series 4 (30% solids)

Figure A.2.3 Particle size distributions for test series 5 (40% solids)

Figure A.2.4 Particle size distributions for test series 6 (35% solids)

Figure A.2.5 Particle size distributions for test series 7 (30% solids)

Figure A.3.1 PSD results for the Malvern and Elzone

Figure A.4.1 Flow-curves of grinding products (35% solids)

Figure A.4.2 Flow-curves of grinding products (30% solids)

Figure A.5.1 Correlation coefficient vs. test number

Figure B.1.1 Particle size distributions for test series 8 (35% solids)

Figure B.1.2 Particle size distributions for test series 9 (35% solids)

Figure B.1.3 Particle size distributions for test series 10 (35% solids)

Figure B.1.4 Particle size distributions for test series 11 (35% solids)

Figure B.1.5 Particle size distributions for test series 12 (35% solids)

List of Tables

Table 2.1 Test program for stirred mill

Table 2.2 Test program for evaluating grinding bead effects on a stirred bead mill

Table 5.1 Relationship between bead diameter (D) and maximum particle size (d) based on geometries shown in Figure 6 where d=2(R/cos 30 –R)

Table A.1 Operating conditions and responses

Table A.6.1. Specific breakage rate

Table A.6.2 Summary of Rheological Test Results

Table A.6.3 Summary of Particle Size Test Results

Table B.2.1 Bimodal bead size composition test

Table B.3.1 Operating conditions and calculations

List of symbols

a	particle size at which 36.8% of particles retained
B_{ij}	primary distribution function
b	size distribution coefficient
D	larger particle diameter
d	small particle diameter
d	bead diameter
GM	grinding media
k	particle size modulus
m	distribution modulus
N_C	media contact number
N_P	number of product particles inside the mill
P_S	probability that a particle is caught and stressed by the media
P_{80}	particle size at which 80% passed
R^2	correlation coefficient
SI	stress intensity
S_j	specific breakage rate of size j
S_1	selection function at 1 mm
SN	stress number
$w_j(t)$	weight fraction of size j material at grinding time t

W_r	Wt. % retained
W	mill hold-up
W_p	Wt % passing
x	particle size
$\hat{\beta}_1$	slope of the fitted regression line
X_i	values of corresponding point X_i
Y_i	values of corresponding point Y_i
$\hat{Y}$	estimated response at X_i based on the fitted regression line
$\overline{Y}$	sample mean of the observations on Y
κ	specific breakage rate
α	coefficient for material characteristics
γ	shear rate
τ	shear stress
τ_{yc}	Casson yield stress terms
τ_{yB}	Bingham yield stress terms
η_C	Casson viscosity terms
η_B	Bingham viscosity terms
η_{ap}	apparent viscosity
ρ	bead density
v_t	bead tangential velocity
Φ	solid volume fraction

Acknowledgements

The great appreciation is given to the Natural Sciences and Engineering Research Council of Canada for the fund and financial support leading to the completion of the research.

Much many thanks are also given to Dr. Bern Klein, for his time and advices on the thesis, and those members of Faculty and Staff, as well as the colleagues at Mining Engineering Department of the University of British Columbia for their kind support and help in my studies during the years of 2001 to 2003.

Chapter 1 Introduction

1.1 Background

Ultra-fine grinding technology in stirred mills has been increasingly applied in mineral processing in recent years due to the increased mineralogical complexity of ores. Specific applications are:

- Poly-metallic sulfide products in flotation cleaning regrind circuits (Enderle et al 1997, Liddel et al 1999);
- Bulk sulfide concentrates containing refractory gold prior to bio-oxidation, pressure oxidation and cyanidation (Liddel et al 1999, Weller etc. 1997);
- Base metal sulfide concentrates prior to pressure leaching and bio-leaching (Liddel et al 1999).

Stirred mills are usually classified into two main groups — vertical and horizontal mills. An industrial scale of the horizontal stirred mills in mineral processing, for example, has been applied successfully in Mount Isa Mine of lead and zinc deposit, Australia. The required grinding product size for liberation of galena requires a P_{80} of 12 μm (Enderle 1997). It was also applied at the McArthur River Mine when it was used to regrind from 30 μm to 7 μm.

Size reduction by grinding accounts for a large proportion of total processing costs due to high energy consumption. Cohen (1983) estimated that typically 30 to 50% of total plant power draw, and up to 70% for hard ores, is consumed by comminution. Since ultra-fine grinding technology is relatively new for metallic ores and deals with very fine particles, greater improvements are needed from grinding control to optimize processing. Such an application

requires a better understanding of the general influence of slurry rheology on breakage kinetics, product size and size distribution, as these parameters affect milling performance greatly in practice. For example, particle breakage kinetics govern mill throughput. The maximum size reduction ratio is expected in single stage of grinding with respect to energy consumption. A narrower size distribution is beneficial to the down stream processes such as flotation and dewatering.

Several studies have been conducted to investigate slurry rheological influences on grinding for both tumbling and stirred mills. The most notable works were by Klimpel and co-workers (1982, 1983, and 1984) for ball and rod mills and Forssberg and his co-workers (1993, 1997) for stirred mills.

Klimpel (1998) conducted extensive laboratory and industrial scale research studies over a twenty-year period on the effects of rheology on grinding. He and co-workers (1982, 1983, and 1984) determined the relationship between the rheological properties and the specific rates of breakage, S_j, and the primary breakage distribution, B_{ij}. They found that "Increasing solid content changed the rheological properties from dilatent to pseudoplastic to yield pseudoplastic", "Slurries exhibiting dilatent behavior give first-order breakage, slurries exhibiting pseudoplastic behavior without a yield value give faster but still first order rates of breakage, and yield value slurries give noticeably slower non-first-order breakage". Based on these findings, slurry solid contents, particle size distributions and chemical environments that maintain pseudoplastic flow behavior provide "optimum" grinding conditions.

The inherent breakage characteristics of the ore also affects the rheology by changing the particle size distribution during grinding. While breakage characteristics cannot be controlled,

other parameters can be adjusted to accommodate these effects. For example, the extent of the pseudoplastic region can be extended by adding dispersing agents (grinding aids) which could improve grinding throughput by up to 15% at the same energy usage (Klimpel 1982, 1983 and 1988).

As stated, Klimpel's research was directed primarily at rod and ball mill grinding in which particles are coarser than in stirred mills. It is believed that the significance of the slurry rheology becomes greater with decreasing particle size since surface chemical particle interactions that contribute to yield stress become increasingly important.

Forssberg and co-workers conducted studies using a pilot scale horizontal stirred mill to grind dolomite and kaolin clays (Gao and Forssberg 1993, Wang and Forssberg 1997). Their results support those of Klimpel, which showed that grinding was "optimum" when the slurry exhibited pseudoplastic flow properties. Their results also indicated that under pseudoplastic rheological conditions, the product particle size distribution was narrower than was obtained when the suspensions exhibited dilatent or yield pseudoplastic properties. Adding polymeric and inorganic dispersants lowered the yield stress, which reduced the energy consumption and produced a narrower and finer product size distribution. The potential to influence particle size distribution by controlling rheology has significant consequences to downstream processes such as flotation, leaching and de-watering. It was therefore an objective of this research to demonstrate more clearly how conditions could be adjusted to affect product size distribution.

In stirred mills, the loading of grinding media usually accounts for about 80% of mill volume. It has been recognized (Stehr et al 1987, Kwade 1999) that the specific energy consumption by stirred mills is less than that of tumbling mills for grinding very fine particles.

Kwade (1999, 2002) assumed that the stress intensity is proportional to the kinetic energy of grinding media, and thus is proportional to both stirrer speed and bead size. The stress number is also proportional to stirrer speed as well as to the number of beads in the mill.

For brittle particles, massive fracture occurs when the overall stress acting on a particle exceeds a critical value resulting in particle disintegration and creating a large number of fragments. Attrition is associated with smaller stresses exerted on particle edges causing a continuous but slow loss of particle mass. It is understood that massive fracture of brittle solids results in faster particle breakage rate than attrition. The size of grinding balls is known to play a very important role in grinding in tumbling mills. In particular, small balls are important for effective compression and attrition of fine particles. It is not clear if this is true for stirred mills. This study was aimed at providing insights into breakage mechanisms in stirred mills and to understand how operating parameters affect them.

Research on the rheology of mineral suspensions has demonstrated that selected compositions of bimodal particle size distributions produce a "minimum" viscosity (Chong, 1971). There is the theoretical possibility of increasing charge mass load while keeping load volume constant by using a selected bead size distribution. The packing density of grinding media can be increased by filling the voids between the largest beads with smaller beads producing a bimodal bead size distribution. The implication is that a bimodal bead size distribution would correspond to a minimum power draw. In practice there is a distribution of bead sizes in grinding mills. During grinding the beads wear reducing their size, which eventually pass through the mill product screen and are rejected. There is a tradeoff between optimizing bead size with respect to grinding (size reduction, power usage, and product size

distribution) and costs associated with media consumption. It is therefore critical to determine the appropriate screen aperture to satisfy both of these criteria.

The above indicates that:

- Rheology determines grinding rate, energy usage and product size distribution, and that pulp density affects these indirectly through its influence on rheology,
- breakage mechanism (s) in stirred mills is not as clear as in tumbling mills,
- bead sizes plays a very important role with respect to the stress intensity and the stress number which are assumed to cause particle breakage in stirred mills.

1.2 Objectives

The objectives of the research are:

- To investigate the breakage kinetics in a horizontal stirred bead mill for the tested slurry rheological properties;
- To characterize the particle size distribution and rheological properties of the grinding pulps for a horizontal stirred bead mill;
- To demonstrate relationship between rheological parameters and ultra-fine grinding with respect to breakage kinetics, product size and size distribution, and power consumption;
- To evaluate the effects of bead size and size composition on breakage rate, product size, size distribution, and grinding power draw.

1.3 Methodology

The research was divided into three main independent but related studies to investigate:

- Particle breakage kinetics
- Rheological effects on ultra-fine grinding
- Effects of bead size on grinding performance

A series of pilot scale grinding tests was designed, and the results obtained from these tests are discussed in Chapter 3, 4, and 5 respectively.

The first part of the research dealt with the particle breakage kinetics in stirred mills as described in Chapter 3. The "one size fraction technique" (Austin 1990) was used to determine disappearance rate of material with time in size fractions. Rosin-Rammler and Gaudin-Schuhmann equations were applied to fit and characterize the product size distributions. Chapter 4 presents the second part of the study which was focused on how slurry rheology affects ultra-fine grinding performance. The flow-curves were modeled using the Casson and Bingham equations to demonstrate the rheological properties of grinding products. The effects of slurry rheology were evaluated using responses such as breakage rate, product size distribution, and the power consumption etc. The third part of the study was the effects of bead size on grinding performance as discussed in Chapter 5. The mill performance was evaluated under different operating conditions with respect to breakage rate, product size distribution, and the power consumption etc. All of these three parts composed of the research.

A Netzsch LME 4 horizontal stirred bead mill was used for the study. The testing was conducted on quartz slurries with varying particle sizes. The mill is a commercial unit that is

applied industrially for ultra-fine grinding of specialized products (pigments). It is also the mill that was scaled–up to develop the ISA mill and is considered suitable for pilot scale studies.

Chapter 2 Experimental Program

2.1 Introduction

The research program was divided into three main parts. Part one focused on the study of fundamental breakage kinetics in horizontal stirred mills (Chapter 3). Part two was aimed at evaluating the influence of slurry rheology on ultra-fine grinding (Chapter 4). Part three dealt with the influences of bead size and bead size composition on stirred mill operation (Chapter 5).

2.2 Experimental System

2.2.1 Equipment and Instruments

Pilot scale tests were conducted using a continuous Netzsch LME 4 horizontal stirred bead mill. The mill is rubber lined and has an effective volume of 2.4 litres. The agitator shaft for the mill has eight polyurethylene discs. The grinding media used were steel beads with the size of 0.5, 1, 2, 3 mm in diameter and the loading charge was 80 % of the total mill volume.

Figure 2.1 is a schematic showing the experimental system that was used. The feed material was mixed in a surge tank (1) and fed to the mill (3) via a positive displacement pump (2). The flow rate was regulated from the control panel (4). The mill is equipped with digital-display panel in which the operating conditions and output parameters (such as agitator and pump speed, mill pressure, temperature, and shaft power) can be monitored and recorded during tests.

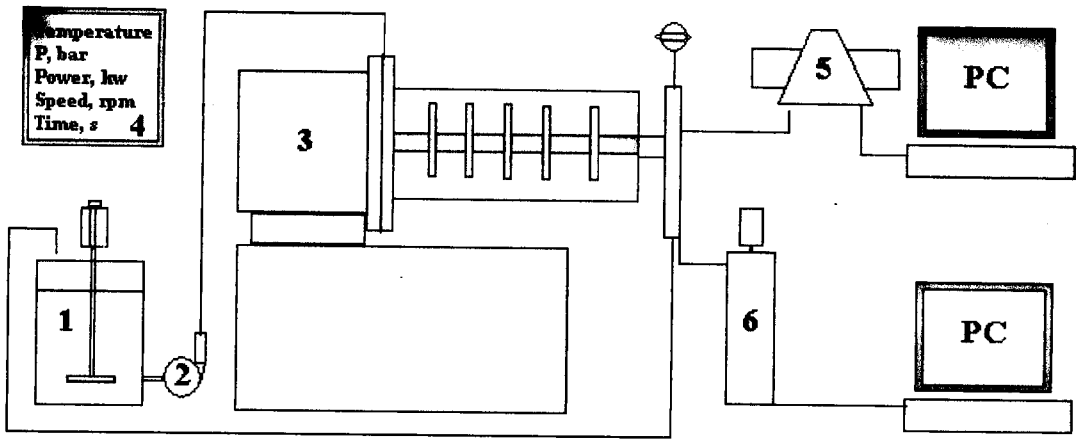

1- Surge tank 2- Pump 3- Netzsch horizontal stirred bead mill 4- Display panel

5- Malvern Mastersizer 6- Haake RV 20 rheometer

Figure 2.1 Experimental system for ultra-fine grinding tests

Particle size analyses were performed using Elzone 280 and Malvern Mastersizer 2000 Laser Diffraction analyzers, with detection ranges of 1to 200 μm and 0.02 to 2000 μm, respectively.

Measuring the rheological properties of mineral suspensions with most viscometers is complicated by errors associated with particle settling, wall slip, non-Newtonian shear rate effects and the onset of turbulence. Klein et al (1995) developed an elongated concentric cylinder fixture for measuring rheological properties of settling suspensions (Figure 2.2) that reduces the significance of these errors. This fixture was used for rheological measurements on all mill products.

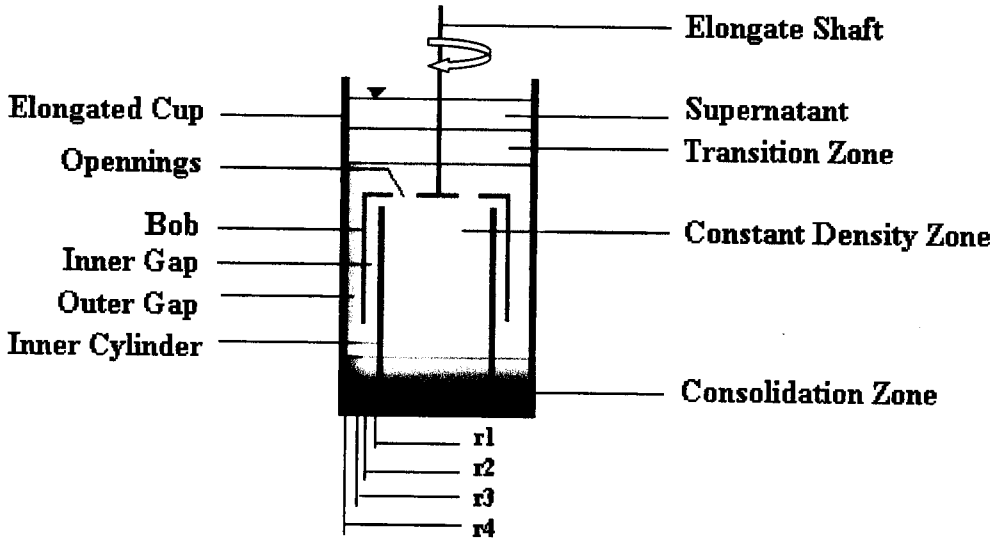

Figure 2.2 Schematic diagram of elongated fixture for rheological measurement of settling suspensions (Klein et al 1995)

2.2.2 Grinding Material

Grinding tests were performed on suspensions of quartz particles with feed sizes (F_{80}) of 83 μm and 32 μm respectively as shown in Figure 2.3.

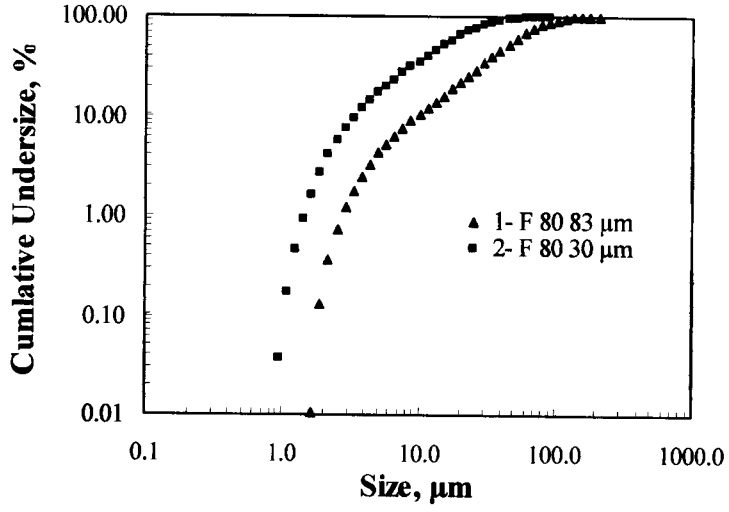

Figure 2.3 Feed size distributions

2.3 Test Design and Procedures

2.3.1 Sampling

Test 1 was conducted to determine the sampling time at which equilibrium conditions are achieved in the mill. Equilibrium refers to stable operation with respect to mill power, temperature and product size (% passing 10 μm). Figure 2.4 plots these parameters versus time and shows that equilibrium is achieved after about 180 seconds; this was therefore used as the minimum operating time before sampling for each test. Sampling involved collecting five cuts from the mill discharge over a period of one minute. The test conditions are shown in Table 2.1.

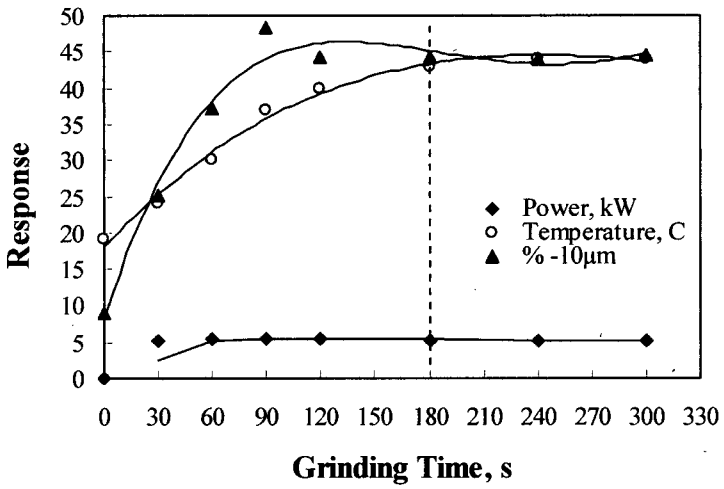

Figure 2.4 Equilibrium test for sampling in the stirred bead mill

2.3.2 Breakage Kinetic Tests

The tests were conducted at three solid contents of 30, 35, and 40% by weight. For each test, a sample was fed to the mill and the product was collected, sampled and re-fed to the mill. This

cycle was repeated up to five times. Between each cycle, the mill was flushed with water before starting the next grinding cycle. Table 2.1 lists the test conditions used for this study.

Table 2.1 Test program for stirred mill

Test No.	Grinding cycles	% Solids	Flow Rate L/Min.	Bead Size mm
1	1	35	3.10	1
2	5	40	1.68	1
3	5	35	1.68	1
4	5	30	1.68	1
5	3	40	3.10	1
6	3	35	3.10	1
7	3	30	3.10	1

Plug-flow was assumed to simplify the calculation of mean residence time, which was defined as the net mill volume divided by the volumetric flow rate. For all tests, the agitator speed was maintained at 1500 rpm. Particle size analyses (PSA) were performed on each product sample using either an Elzone 280 or a Malvern Mastersizer 2000 Laser Diffraction. The particle size and size distributions were determined for each residence time. The disappearance rate of the top narrow size fraction of the feed slurries was obtained and calculated, and the breakage rate of this size fraction was plotted against the particle residence time.

The feed material used in this study was quartz with an F_{80} of 83 μm.

2.3.3 Rheology Tests

The tests for evaluating slurry rheological influences on stirred mills were conducted in the same plan and procedures as shown in Table 2.1. In addition, the rheological properties for each grinding product sample were determined using a Haake RV 20 rheometer shown in Figure 2.2.

2.3.4 Bead Size Tests

Grinding tests were performed on suspensions of quartz particles with feed sizes (F_{80}) of 83 μm and 32 μm (Figure 2.3). The feed slurry solid content was maintained at 35% solids by weight. Test conditions are shown in Table 2.2. The slurry feed rate was kept constant at 3.1 l/min. For test with constant agitator speed (1500 rpm), the power usage was recorded as a response. For test with constant power, the agitator speed was adjusted to maintain this constant power and recorded. For tests with bimodal bead sizes, a series of tests were performed using varying proportions of small beads (zero to 100%).

Table 2.2 Test program for evaluating grinding bead effects on a stirred bead mill

Test No	Feed Size F_{80} μm	Agitator Speed rpm	Pump Flow Rate L/Min	Agitator Power kW	Bead Size mm
8	30	1500	3.1	—	0.5, 1, 2, 3
9	83	—	3.1	3.7	0.5, 1, 2, 3
10	30	—	3.1	3.7	0.5, 1, 2, 3
11	83	1500	3.1	—	0.5+2
12	83	—	3.1	3.7	0.5+2

Chapter 3 Particle Breakage Kinetics in Horizontal Stirred Mills

3.1 Introduction

The objectives of this part of the research were to investigate breakage kinetics and characterize particle size distributions for stirred mills.

The particle breakage kinetics, product size and size distribution, grinding limit and mechanisms for quartz suspensions in a horizontal stirred mill were investigated and discussed. The product size distributions from stirred mill were fitted using the Rosin-Rammler and the Gaudin-Schuhmann equations, and the fitted results were compared.

A method of determining breakage rates versus particle size was demonstrated and the 10% top size fraction was recommended for the determination of specific breakage rates.

3.2 Literature Review

Stirred bead mills have been applied increasingly to ultra-fine grinding of minerals. However, since stirred mills have only recently been introduced to large-scale metal mines, models have not been developed to the same degree as for tumbling mills.

The most popular mathematical model used for tumbling mills is the "population balance model", which was introduced by Epstein (1947), and developed further by several researchers (Whiten 1974, Herbst and Fuerstenau 1968, 1973, Austin et al 1983). For this model, a "first order breakage rate" is assumed. First order breakage is based on the hypothesis that for a given

size range of particles, for example a $\sqrt{2}$ screen interval, the production of ground material per unit time within the mill depends only on the mass of that size fraction which is present in the mill contents (Austin, 1990).

$$\text{Breakage rate of size fraction } j = S_j\, w_j(t)\, W \qquad (3.1)$$

Where, S_j is the specific breakage rate of size j,

W is the mill hold-up,

$w_j(t)$ is the weight fraction of size j material at grinding time t.

Thus,

$$dw_j(t)/dt = -S_j w_j(t) \quad \text{or} \quad w_j(t) = w_j(0)\, e^{-Sj\,(t)} \qquad (3.2)$$

For a batch mill the population mass balance equation is:

$$dw_i(t)/dt = -S_i w_i(t) + \sum_{\substack{j=1 \\ i>1}}^{i-1} b_{ij}\, S_j w_j(t) \qquad \text{where } n>i>j>1 \qquad (3.3)$$

Where, b_{ij}, is the primary breakage distribution function.

The primary breakage distribution function describes the weight fraction of the products that occur in the size interval i if material of size interval j is broken. Equation (3.3) states that the net rate of production of size i material equals the sum of the rates of appearance from breakage of all sizes larger than size i minus the rate of disappearance of size i by breakage. Morrell et al (1993) developed a population balance model for tower mills, which are similar to horizontal stirred mills.

Hogg (1999) developed a theoretical model for the breakage kinetics for stirred mills that accounts for breakage by massive fracture and attrition. He suggested that attrition becomes more important as particles become finer, particularly in the micron range. His model indicates that attrition grinding results in acceleration of particle degradation and non-first-order breakage. In this case, the population-balance equation could not be applied to stirred mill grinding.

Studies were conducted with a pilot scale horizontal stirred mill to characterize the particle breakage kinetics. In particular, the study was aimed at determining whether or not first-order breakage occurs such that the population balance model could be applied. The results were analyzed to provide evidence of the types and relative magnitudes of particle breakage mechanisms.

3.3 Procedures

The test procedures were described in details in Chapter 2 (test 2 to test 7).

3.4 Results and Discussion

3.4.1 Product Size Distribution

The Gaudin-Schuhmann (Equation 3.4) and Rosin-Rammler (Equation 3.5) equations were used to characterize the particle sizes of the grinding mill products.

Gaudin Schuhmann

$$W_p = 100\,(x/k)^m \tag{3.4}$$

Where, W_p is Wt % passing,

x is the particle size,

k is the particle size modulus,

m is the distribution modulus.

Rosin-Rammler

$$W_r = 100 \exp\,[-(x/a)^b] \tag{3.5}$$

Where, W_r is Wt. % retained,

x is the particle size,

a is the size at which 36.8% of particles retained,

b is the distribution coefficient.

The model fits were compared using the correlation coefficient R^2, which is defined as follows:

$$\hat{Y} = \hat{\beta}_0 + \hat{\beta}_1 X_i \tag{3.6}$$

$$R^2 = \frac{\sum_{i=1}^{n}(Y_i - \bar{Y})^2 - \sum_{i=1}^{n}(Y_i - \hat{\beta}_0 - \hat{\beta}_1 X_i)^2}{\sum_{i=1}^{n}(Y_i - \bar{Y})^2} \tag{3.7}$$

Where $\hat{\beta}_0$ is the intercept of the fitted regression line,

$\hat{\beta}_1$ is the slope of the fitted regression line,

X_i and Y_i are the values of corresponding point (X_i, Y_i),

$\hat{Y}$ denotes the estimated response at X_i based on the fitted regression line,

$\overline{Y}$ is the sample mean of the observations on Y.

The correlation coefficient R^2 was plotted against test number (Figure 3.1) for both Equations. The average correlation coefficient R^2 for the Gaudin-Schuhmann and Rosin-Rammler equations were 0.88 and 0.97, respectively. The results suggest that the Rosin-Rammler fits the data better than Gaudin-Shuhmann model. Therefore the Rosin-Rammler equation was used to characterize the size distribution of the feed and stirred mill products.

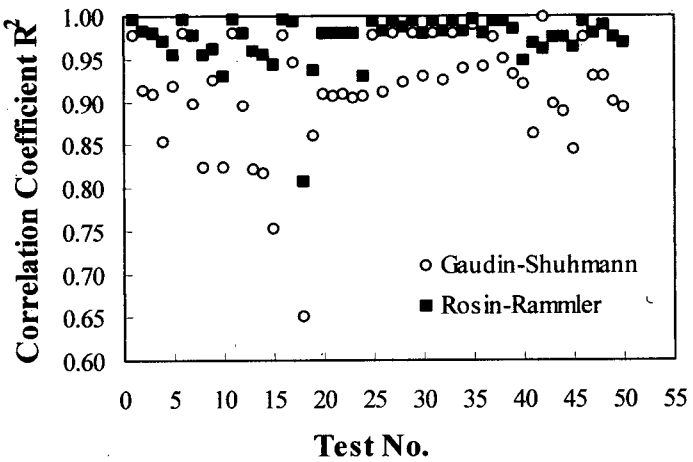

Figure 3.1 Correlation coefficient of both fitted models vs. test number

In order to assess the suitability of the Rosin Rammler equation over the range of particle sizes and size distributions, the correlation coefficient R^2 was plotted against the product size (P_{80}) and distribution coefficient (b). The trend lines shown in Figures 3.2 and 3.3 reveal that

Rosin Rammler equation fits the data best at coarser sizes and at narrower size distributions (higher values of b).

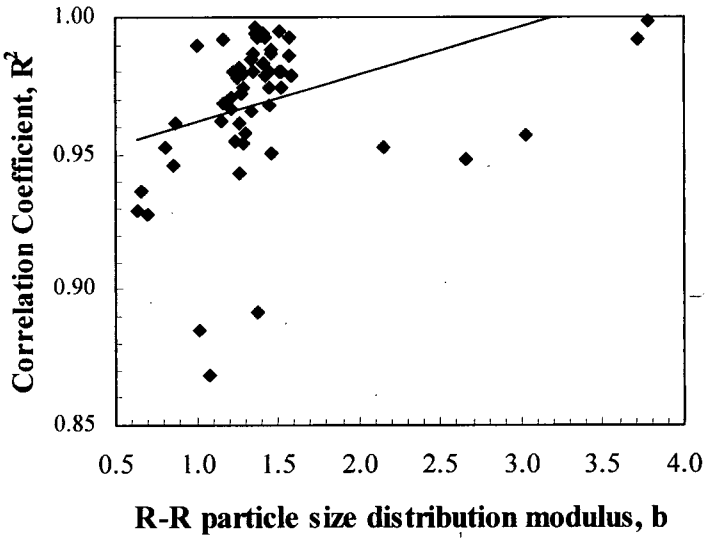

Figure 3.2 Relationship between distribution modulus and correlation coefficient

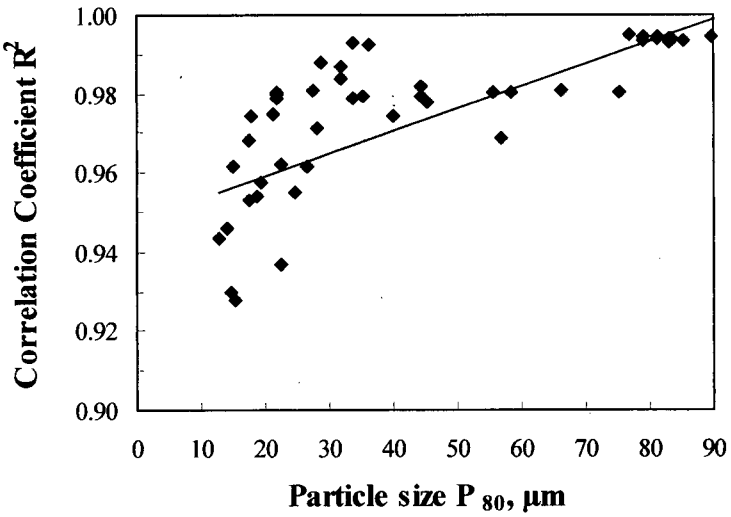

Figure 3.3 Relationship between particle size and correlation coefficient

Figure 3.4 is a plot of size distribution modulus versus product size. The graph indicates that the size distribution becomes narrower (b increases) with decreasing product size P_{80}. The trend

Rosin Rammler equation fits the data best at coarser sizes and at narrower size distributions (higher values of b).

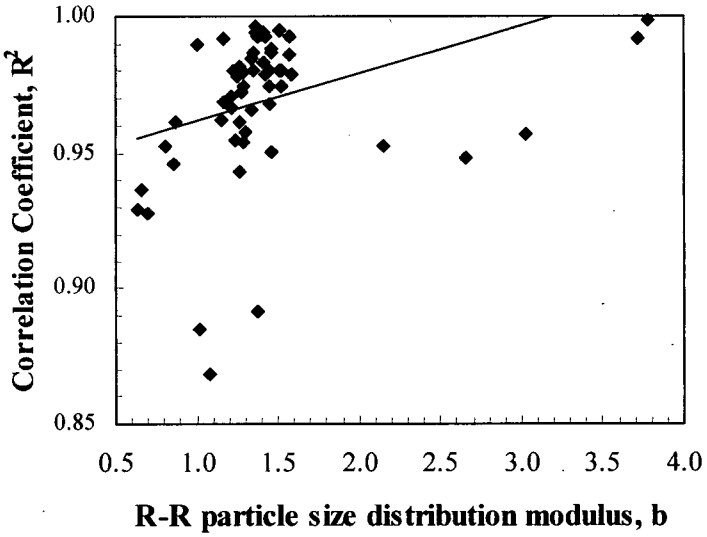

Figure 3.2 Relationship between distribution modulus and correlation coefficient

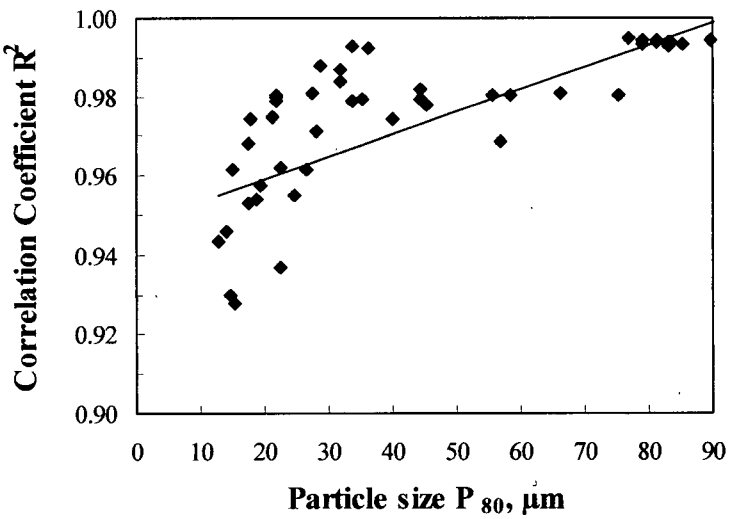

Figure 3.3 Relationship between particle size and correlation coefficient

Figure 3.4 is a plot of size distribution modulus versus product size. The graph (refer to tests from 2.1 to 4.5 in table A.6.3, Appendix A) indicates that the size distribution becomes narrower

(b increases) with decreasing product size P_{80}. The trend becomes more significant with decreasing solid content. The results imply that decreasing the solid content will produce a narrower size distribution.

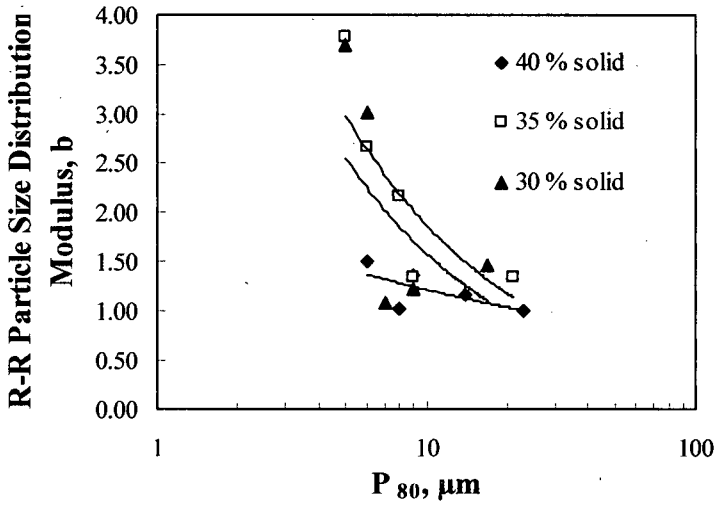

Figure 3.4 Rosin-Rammler particle size distribution modulus versus product size P_{80}

Figure 3.5 shows the size distribution of the mill feed sample, which is characterized by a size coefficient of 53.92 and distribution coefficient of 1.38. Figure 3.6 shows the fitted Rosin-Rammler equation through five cycles of grinding in the stirred mill for test number 2. Examination of the fitted Rosin-Rammler equation reveals a reasonable fit down to about 3 µm, below which it deviates from the data.

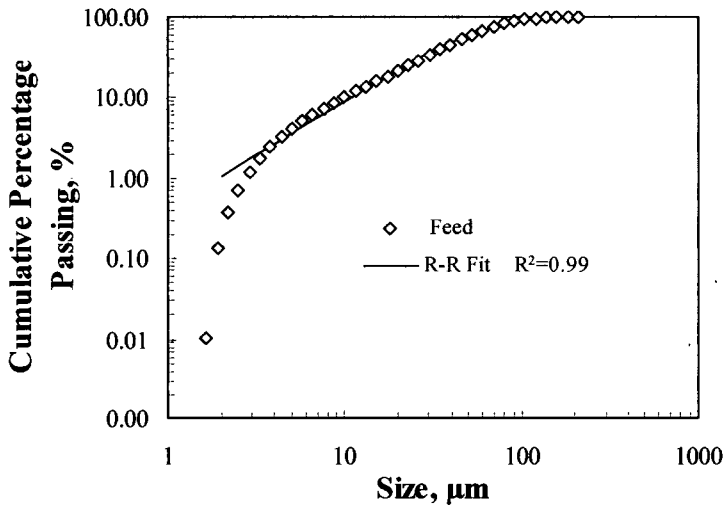

Figure 3.5 Particle size distribution of feed sample with fitted Rosin Rammler equation

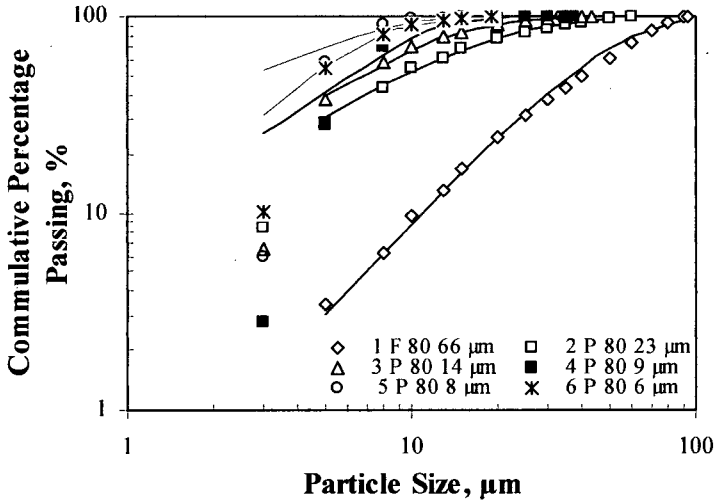

Figure 3.6 Particle size distribution products from five cycles of grinding with fitted Rosin-Rammler equation

3.4.2 Breakage Rate

The "one size fraction technique" (Austin 1990) was used to determine the disappearance rate of the top narrow size fraction of the stirred mill feed. The specific breakage rates S_j were then obtained from plots of breakage rate w (t) versus particle residence time t:

$$\text{Log } w(t) = \text{Log } w(0) - S_j\, t/2.3 \qquad (3.8)$$

The breakage rates were determined for two size fractions, the +97 μm fraction and the +64 μm fraction. The tests were conducted at three solid contents of 30, 35 and 40%.

Figures 3.7 and 3.8 show the relationship between particle breakage rate and residence time. The slope of each line represents the specific breakage rate S_j. The linear relationship suggests "first-order" particle breakage in the mill. Since first order breakage is observed for the two different size fractions, it is assumed that all size fractions will experience first order breakage. The curves show that breakage rate increases with decreasing solid content. By comparing Figure 3.7 and 3.8 it can be seen that the breakage-rate decreases with decreasing particle size. At 30% solids the specific breakage rate (slope of the line) for the 97 μm fraction is 0.048 as compared to the rate for the 64 μm fraction, which is 0.038.

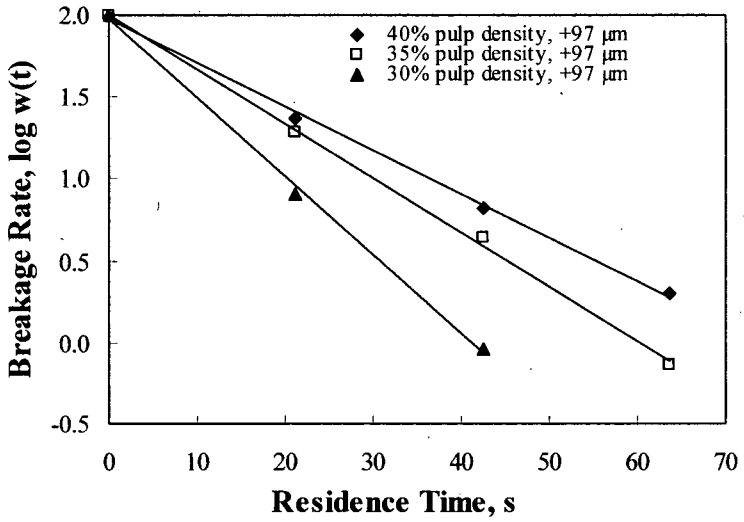

Figure 3.7 Breakage rate versus grinding time for the +97 µm fraction

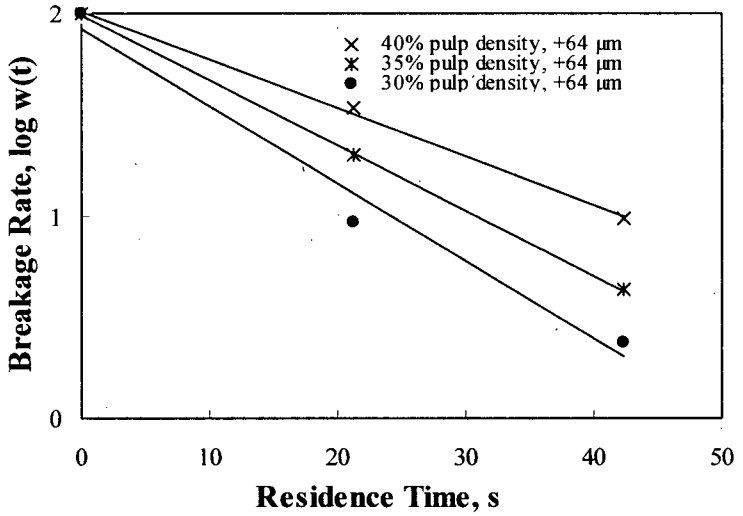

Figure 3.8 Breakage rate versus time for the +64 µm fraction

The results confirm "first-order" breakage rates for stirred mill grinding and support the use of the population balance model. As described by Hogg (1999), attrition breakage would lead to the acceleration of the disappearance and appearance resulting in non-first-order breakage. Therefore the 'first order' breakage rate implies massive fracture breakage mechanisms for the operating conditions used in this study.

Kwade (1999) analyzed the bead trajectories and power density zones for a stirred disc mill. He concluded that stress resulting from bead collision (impact) is the main mechanism causing particle breakage in stirred mills, as long as the particle size is larger than 1 μm and the solid concentration is not too high. Breakage resulting from bead collision would lead to fracture rather than attrition, supporting results that suggest attrition plays a minor role in stirred mill grinding.

3.4.3 Breakage Rate versus Particle Size

For determination of specific breakage rate using the "one size fraction technique", 5, 10, and 20 % were chosen as top size fractions for the particle size distributions of grinding products from the mill. A set of grinding results for different top size fractions were obtained as shown in Figure 3.9. Since the conventional sieve order is not appropriate for determination of the top size fraction in such fine particle sizes studied, the problem could be solved by applying percentiles of oversize particles as top size fractions which could be easily determined using Malvern Mastersizer 2000. The following work was to test and choose an appropriate percentile for the purpose. The top size fraction w(0) of each grinding product was determined and w(t) was obtained from a successive grinding products through a series of grinding tests using both Malvern Mastersizer 2000 and Equation (3.8). Since first-order breakage rate was confirmed, the specific breakage rate could be obtained by the slope of a two point line.

As shown in Figure 3.9, the results of specific breakage rate with 5% top size fraction show significant variation as indicated by the low R^2 value of 0.95. The variation can be explained by variable composition of the material in the 5% top size fraction, which is not representative. Using a top size fraction of 20% shows same variation indicated by a R^2 value of 0.97. This is

likely due to particle breakage overlap (i.e. top size particle create progeny that are still within the upper 20% range). It is suggested that the 10% top size fraction of the grinding products in stirred mills is the most appropriate in that it does not suffer from variable composition or breakage overlap. This is supported by the R^2 value of 0.99.

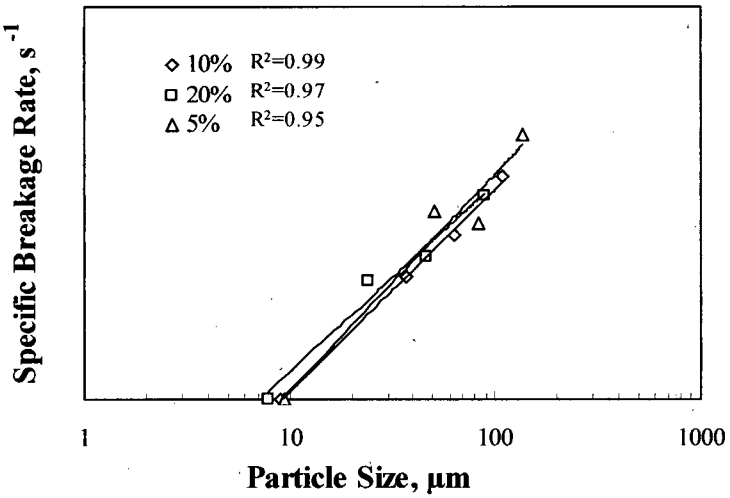

Figure 3.9 Specific breakage rate vs. top particle size fractions representing 5, 10 and 20 percentiles

Figure 3.10 shows a good linear relationship between specific breakage rate and particle size for a stirred mill. The curve shows the same type of relationship found for ball mills; a decrease in breakage rate as feed size become smaller. The straight line portion of the Austin model can be used to describe the results for the specific breakage rate – particle size relationship.

$$k = S_1 d_p^{\alpha} \qquad (3.9)$$

S_1 is the selection function at 1 mm and was determined to be 0.0035. The slope of the line is α, which is 0.51.

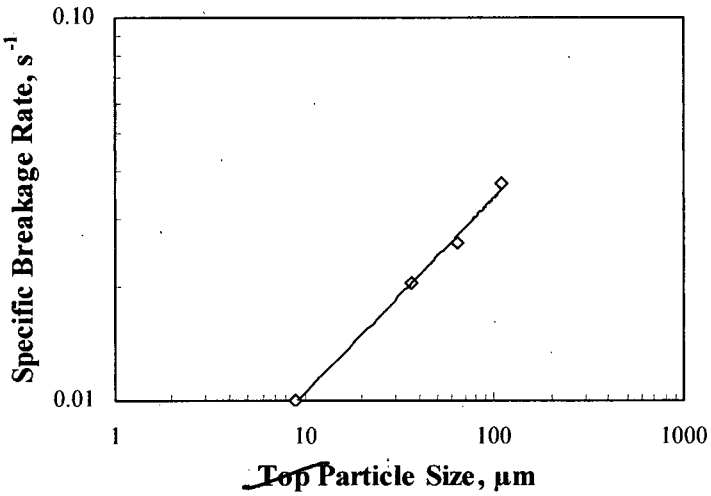

Figure 3.10 Specific breakage rate vs. top particle size fraction

3.4.4 Grinding Limit

The size reduction ratio was also determined from the five cycle grinding tests. The size reduction ratio refers to the ratio of feed size to product size for each cycle (F_{80} /P_{80}). Figure 3.11 shows that the size reduction ratio decreases with the feed size and approaches 1.0 at about cycle five. A value of 1.0 indicates that, for the grinding condition tested, a grinding limit exists whereby increasing grinding time no longer results in particle breakage. The existence of a grinding limit is supported by the shape of the product size distribution curves, which drop off sharply below about 3 µm; this is where the Rosin Rammler equation deviates from the data.

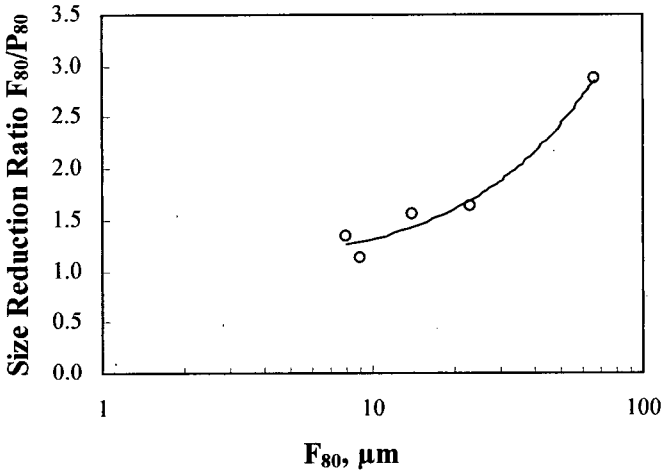

Figure 3.11 Particle size reduction ratio versus feed size F_{80}

Tromans and Meech (2002) conducted a theoretical study of fracture toughness and surface energies. Based on their results, it is suggested that the grinding limit depends on the square of the critical stress intensity for crack propagation, provided that the energy is effectively exerted on to the particles. It is reasonable to consider that more energy will be needed to fracture a particle that lacks flaws. They also calculated the energy efficiency (theoretical computed value over Bond Work Index) for many minerals, and showed that all the energy efficiencies are very low (of the order of 1 %). The low efficiency was attributed to energy losses due to particle deformation and to inefficient impact from grinding media. Therefore during mill operation, it seems that the practical grinding limit depends on the effective stresses created in the mill rather than critical stress intensity for crack propagation for a material. The limit observed from the tests (Figure 3.11) is likely a limitation of mill conditions rather than the material itself.

3.4.5 Breakage Mechanisms

Attrition and abrasion (no impact) were once believed to be the primary breakage mechanisms in stirred bead mills. Recent observations (Kwade 1999, 2002, Shinohara et al 1999) suggest that all three breakage mechanisms (attrition, abrasion and impact) exist in these mills, although the degree may vary from case to case.

Hogg (1999) assumed that product size would become increasingly bimodal as the relative contribution from attrition increases. Figure 3.12 shows the size distribution of products through three successive cycles of grinding. For cycles one and two, the distribution becomes narrow as the grinding limit is approached. Cycle 3 results in the production of a very fine fraction of about 0.2 μm in size creating a bimodal size distribution. The results suggest that massive fracture was the main breakage mechanism from cycles one and two. However, near the grinding limit, attrition becomes dominant and there seems to be very little massive fracture.

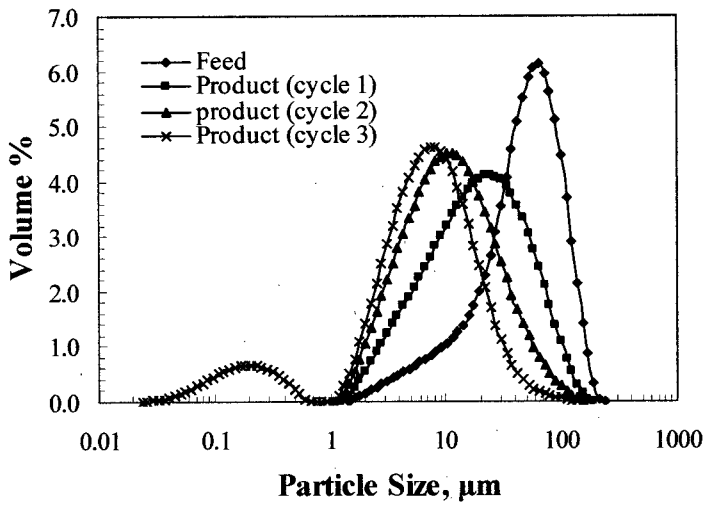

Figure 3.12 Particle size distributions of stirred mill products following successive grinds

3.5 Conclusions

The breakage kinetics of quartz suspensions with different solid content were investigated for a horizontal stirred bead mill. The results show that the Rosin-Rammler fits the data better than Gaudin-Shuhmann equation. The Rosin-Rammler fit improves for products with a narrower size distribution and coarser particle size but is poor for particle sizes below about three microns. It is also shown that decreasing the solid content will produce a narrower size distribution.

The results confirm the "first-order" breakage rate for tested slurries in the mill. The 'first order' breakage rate implies massive fracture breakage mechanisms for the operating conditions used in this study. The breakage rate increases with decreasing solid content.

A method of determining breakage rates versus particle size is demonstrated which is based on Austin's "one size fraction technique". Results show that the 10% top size fraction is most appropriate for the determination of specific breakage rates in a stirred mill. The breakage rate decreases as the particle size becomes finer.

The size reduction ratio decreases with the feed size and approaches 1.0, indicating that a grinding limit exists. The practical grinding limit depends on the effective stresses created in the mill rather than critical stress intensity for crack propagation for a material. The limit observed is likely a limitation of mill conditions rather than the material itself.

Based on size distribution results, the primary breakage mechanism in the horizontal stirred mills is massive fracture. However, near the grinding limit attrition becomes dominant.

3.6 Recommendations

The breakage kinetics was investigated and modeled using Austin's "first order" breakage model for a stirred mill. The study is only part of the modeling work. Further work needs to be done on the primary distribution function modeling for the products from stirred mills so that the population mass balance model can be fit and the characteristics (particle size and size distribution) of products from stirred mill can be predicted.

It was confirmed that bimodal distributions of grinding products occur as particle sizes become finer in the study when a very fine fraction is generated through attrition. For optimization of ultra-fine grinding, it is necessary to investigate further the critical operating conditions for stirred mill to limit the production of very fine particles which may not favor down stream processes such as flotation and dewatering.

Chapter 4 Rheological Effects on Ultra-fine Grinding in Stirred Mills

4.1 Introduction

The rheological properties of stirred mill pulps with varying solid content, particle size and size distribution were determined and modeled using the Casson and Bingham flow-curve equations. The objectives of the research were:

a) To characterize the rheological properties of the grinding pulps from a horizontal stirred bead mill.

b) To investigate the breakage kinetics in a horizontal stirred bead mill for the tested slurry rheological properties.

c) To demonstrate relationship between rheology and grinding kinetics.

d) To investigate the relationship between rheological parameters and slurry parameters such as particle size (P_{80}), size distribution and solid content.

e) To demonstrate the influence of rheological parameter (s) on fines (-10 μm) production, product size distribution and grinding power consumption.

4.2 Literature Review

Rheology describes the relationship between shear stress and shear rate for fluids and slurries. There are several common shear stress–shear rate relationships that are characterized by flow-curves as shown in Figure 4.1. Fluids such as water or oil exhibit Newtonian flow properties which are characterized by a single parameter, the viscosity which is the slope of the flow curve. Mineral suspensions exhibit non-Newtonian flow properties, for which a single viscosity term does not adequately describe the flow properties. Apparent viscosity can be used to characterize

the non-Newtonian rheology of slurries if the "characteristic" shear rate for the process is known. The apparent viscosity is the slope of a line that passes through the origin and intersects the flow curve at the specified "characteristic" shear rate.

Several studies have been conducted to optimize stirred mill performance as a function of feed rate, stirrer speed, ball charge, ball size, ball density and other parameters (Gao, Forssberg, and Weller 1996, Tuunila and Nystrom 1997, Yan, Dunne and Freeman 1995). Relatively few investigations have been conducted to evaluate rheological aspects of grinding in these types of mills. The most notable was by Forssberg and his co-workers (Gao and Forssberg 1993, Wang and Forssberg 1997).

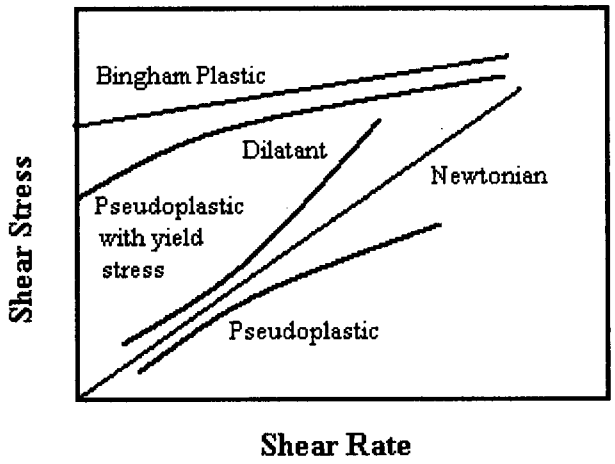

Figure 4.1 Common rheological flow-curves

Klimpel (1998) conducted extensive laboratory and industrial scale research studies over a twenty-year period on the effects of rheology on grinding. They found that increasing solid content changed the rheological properties from dilatent to pseudoplastic to yield pseudoplastic. The solid content at which the rheological properties changed was dependent on other slurry

properties such as particle size distribution, breakage characteristics of the material and chemical environment (Klimpel 1988).

Klimpel and co-workers (1982, 1983, and 1984) determined the relationship between the rheological properties and specific rates of breakage parameters, S_j, and primary breakage distribution parameters, B_{ij}. The first-order breakage model can be expressed as:

$$w_j(t) = w_j(0)\, e^{-Sj\,(t)} \qquad (4.1)$$

Where S_j is the specific breakage rate of size j,

$w_j(0)$ is the weight fraction of size j material at grinding time 0,

$w_j(t)$ is the weight fraction of size j material at grinding time t.

Specifically, "slurries exhibiting dilatent behavior give first-order breakage, slurries exhibiting pseudoplastic behavior without a yield value give faster but still first order rates of breakage, and yield value slurries give noticeably slower non-first-order breakage" (Klimpel 1998). Based on these findings, slurry solid contents, particle size distributions and chemical environments that maintain pseudoplastic flow behavior provide "optimum" grinding conditions.

The inherent breakage characteristics of the ore also affect the rheology by changing the particle size distribution during grinding. While inherent breakage characteristics cannot be controlled, other parameters can be adjusted to accommodate these effects. The extent of the pseudoplastic region can be extended by adding dispersing agents (grinding aids) which could improve grinding throughput by up to 15% at the same energy usage (Klimpel 1982, 1983 and 1988).

Klimpel's research was directed primarily at rod and ball mill grinding in which particles are coarser than in stirred mills. It is believed that the significance of the slurry rheology becomes greater with decreasing particle size since surface chemical interactions that contribute to yield stress become increasingly important.

Forssberg and co-workers conducted studies using a pilot scale horizontal stirred mill to grind dolomite and kaolin clays (Gao and Forssberg 1993, Wang and Forssberg 1997). Their results support those of Klimpel, which showed that grinding was "optimum" when the slurry exhibited pseudoplastic flow properties. Their results also indicated that under pseudoplastic rheological conditions, the product particle size distribution was narrower than was obtained when the suspensions exhibited dilatent or yield pseudoplastic properties. Adding polymeric and inorganic dispersants lowered the yield stress, which reduced the energy consumption and produced a narrower and finer product size distribution. The demonstrated potential to influence particle size distribution by controlling rheology has significant potential consequences to downstream processes such as flotation, leaching and de-watering.

Velamakanni and Fuerstenau (1993) found that a polymeric dispersant can significantly affect slurry viscosity only at a high solid content, appropriate pH and an over critical dosage. Proper polymer usage resulted in a more finely ground product in the laboratory ball mill.

Napier-Munn and Shi (1996) conducted forty-five surveys on sixteen industrial ball mills in five industrial sites. They concluded "the slurry encountered in mineral processing can exhibit a wide range of rheological properties, which affect process performance significantly; some times in a non-intuitive way." This conclusion explains why observations from different researchers

can vary widely. For example, Kapur et al (1996) suggested that the stirred mill product size distribution are essentially identical self-similar curves when particle size is rescaled by dividing by the median size irrespective of the presence or absence of dispersants. They concluded that neither grinding mechanisms nor grinding rate is altered by the presence of dispersants. These results contradict those of Klimpel and Forsberg and suggest that it is not possible to alter conditions to affect particle size distribution.

The results of grinding studies demonstrate that rheology, not pulp density determine grinding rate, energy usage and product size distribution. However, there are some contradictions in published information regarding the effects on grinding. Therefore, it is essential to investigate how slurry rheology affects particle breakage kinetics, fines production, particle size and size distribution, as well as the power consumption in a stirred mill. This study was conducted to increase our knowledge of the effect of rheology, specifically with respect to grinding in horizontal stirred mills.

4.3 Procedures

The test procedures were described as shown in Chapter 2 (test 2 to test 7) for this part.

4.4 Results and Discussions

4.4.1 Flow-Curve Modeling

The rheological data for the grinding products were fitted using both Casson and Bingham flow-curve equations (Equation 4.2 and Equation 4.3). These models are simple two parameter

equations, whose coefficients have physical significance. Both equations have a yield stress term that represents the threshold amount of stress to initiate flow. The viscosity coefficient in each equation is approached by the high shear rate apparent viscosity. Both equations collapse to the equation for a Newtonian fluid as the yield stress approaches zero.

$$\text{Casson} \quad \tau^{1/2} = \tau_{yC}^{1/2} + (\eta_C \gamma)^{1/2} \tag{4.2}$$

$$\text{Bingham} \quad \tau = \tau_{yB} + \eta_B \gamma \tag{4.3}$$

Where,

τ is the shear stress,

γ is the shear rate,

τ_{yC} and τ_{yB} are yield stress terms,

η_C and η_B are viscosity terms

Examination of the shape of the flow-curves presented in Figure 4.2 reveals that the suspensions are almost Newtonian at coarse particle sizes. As particle size decreases they become increasingly pseudo-plastic and eventually yield pseudo-plastic. Over the range of conditions studied in this research, dilatant properties were not observed, which contrasts results from other grinding studies (Klimpel 1982, 1983).

Figure 4.2 shows the fits with Casson equation and Figure 4.3 shows the fits using Bingham equation. It is evident that Casson equation fits the data better than Bingham equation, particularly at low shear rates. The correlation coefficient R^2 was used as a criterion to compare

the equation fits. The average R^2 values for the Casson and Bingham plastic equations are 0.98 and 0.93 respectively, supporting the selection of the Casson equation.

Gao and Forssberg (1993) investigated the rheological behavior of dolomite slurries in a horizontal stirred bead mill. They characterized the slurry flow curves as Bingham plastic by linearly extrapolating the high shear rate data. As demonstrated by the graphs, such a straight line extrapolation can over estimate the magnitude of the yield stress.

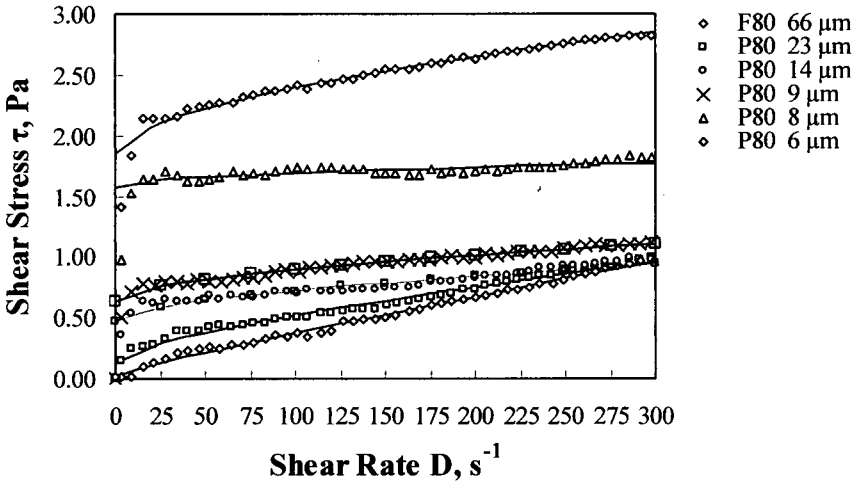

Figure 4.2 Flow-curves of fine quartz suspension (Casson Fitted, 40% Solids)

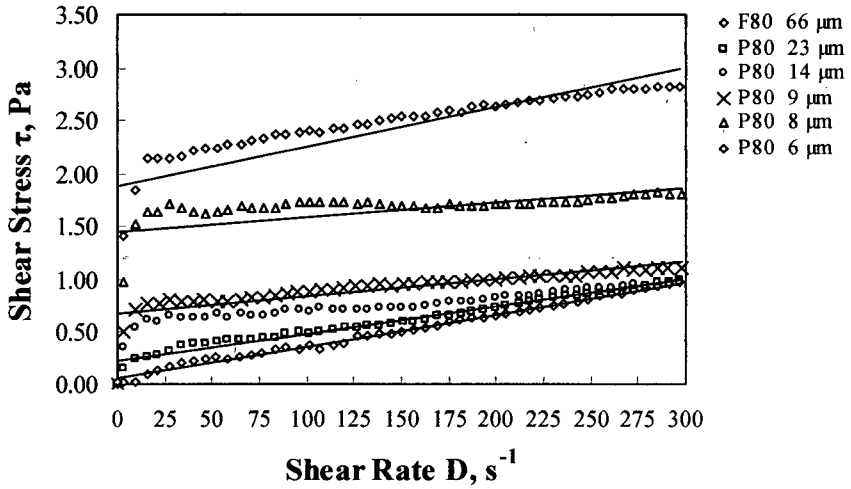

Figure 4.3 Flow-curves of quartz suspension with Bingham fitting (40% solids)

4.4.2 Effect of Solid Content and Particle Size

All slurry products were modeled using the Casson equation. The equation coefficients (τ_{yc}, η_c) were then related to particle size and solid content. Figures 4.4 and 4.5 show the relationship between the yield stress, solid content and particle size.

At 30% solids, the influence of particle fineness on slurry rheology is negligible. As the solid content increases to 35%, the yield stress variation becomes evident but the influence from particle fineness on yield stress is still relatively small. Increasing the solid content further, to 40%, results in a more significant change in the slurry yield stress. As particles become smaller, this change becomes larger. This result agrees well with observations by Gao and Forssberg (1993). In some of their tests the agitator stopped running due to the increased yield stress during grinding at very fine sizes.

It is well known that yield stress will increase exponentially above a critical solid content. The results suggest the critical solid content is between 35% and 40% solids by weight. As particles become smaller the critical solid content decreases. For example, assuming a critical yield stress of 0.1 Pa, the critical solid content at a P_{80} of 7μm is about 35% solids and at 25 μm is about 40% solids (Figure 4.4).

The results demonstrate how solid content and particle size interact to affect the slurry rheological behavior. It is obvious that the rheological properties are not only determined by solid content, but also by other physical characteristics (particle size) as well.

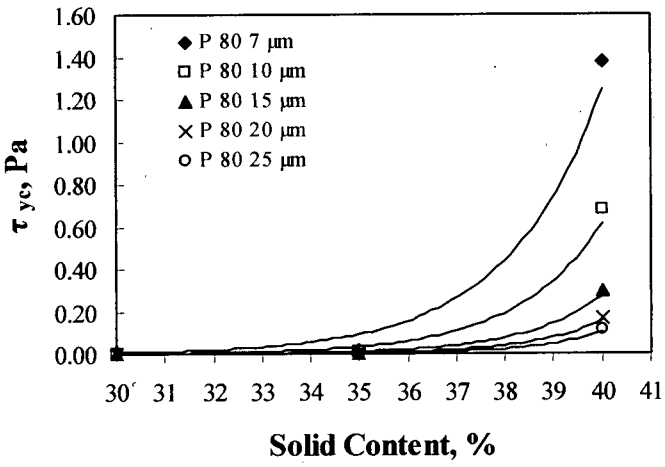

Figure 4.4 Yield stress vs. solid content of slurries tested

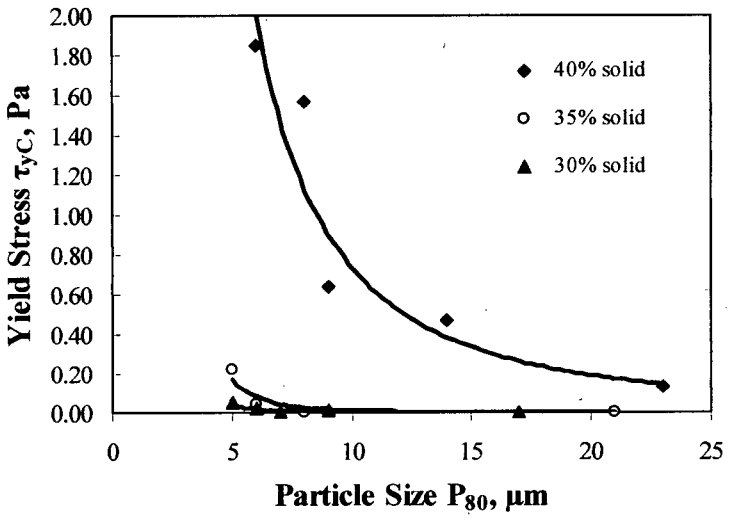

Figure 4.5 Yield Stress vs. Particle size

Apart from the yield stress, the Casson viscosity was also plotted against solid content and particle size in Figures 4.6 and 4.7. The trend lines in Figure 4.6 indicate that the Casson viscosity decrease with increasing solid content which contradicts the expected relationship. Figure 4.7 shows that the influence of particle size on the Casson viscosity is negligible at 30 to 35% solids. However, unlike the yield stress, the viscosity data are relatively scattered (R^2 from 0.62 to 0.75) and the influence is quite weak (the scale is in mPa.s).

In order to interpret these results, Figures 4.8 and 4.9 were plotted to show the relationship between apparent viscosity (at shear rate of 50 and 300 s^{-1}) and particle size. The apparent viscosity varies with particle sizes only at 40% solid content, and increases as the particle sizes become smaller. The results are similar to those obtained in Figures 4.4 and 4.5 for yield stress. The similarity suggests that yield stress is the dominant rheological parameter that contributes most to the apparent viscosity. The trend of decreasing the Casson viscosity with solid content seems to be an artifact of the equation fits and the magnitude is negligible.

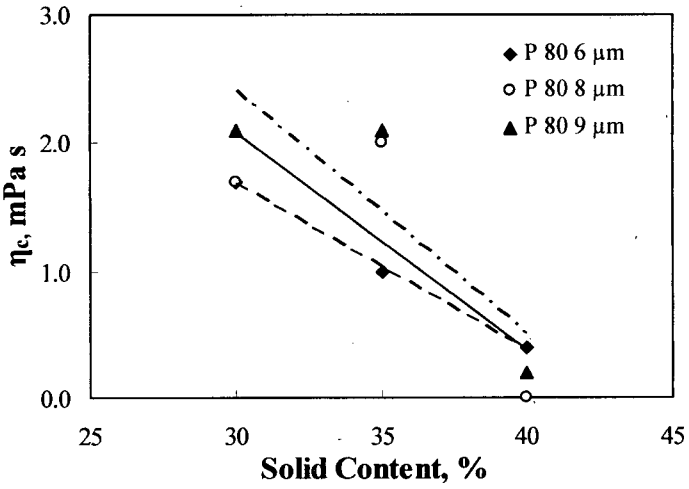

Figure 4.6 The Casson viscosity vs. solid content

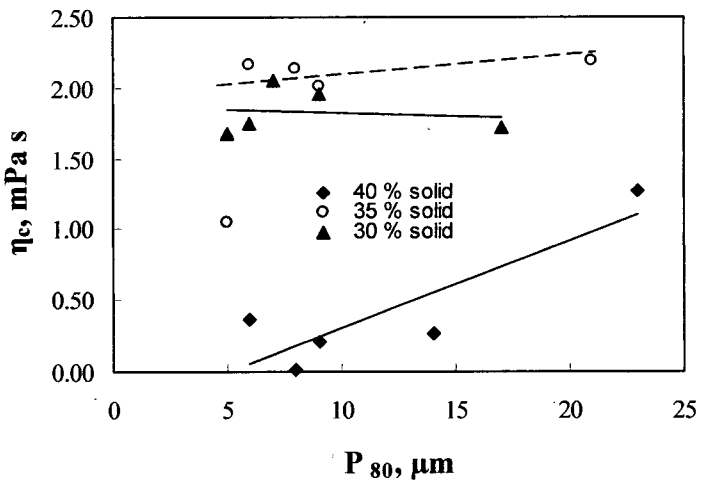

Figure 4.7 The Casson viscosity vs. particle size P_{80}

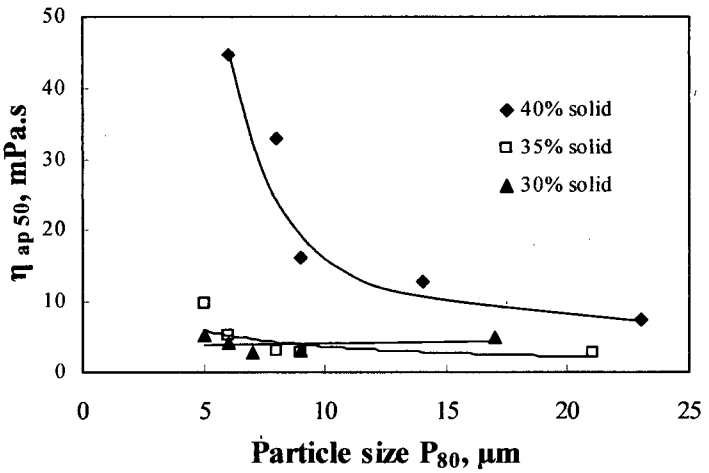

Figure 4.8 Apparent viscosity (50 s^{-1}) vs. particle size P_{80}

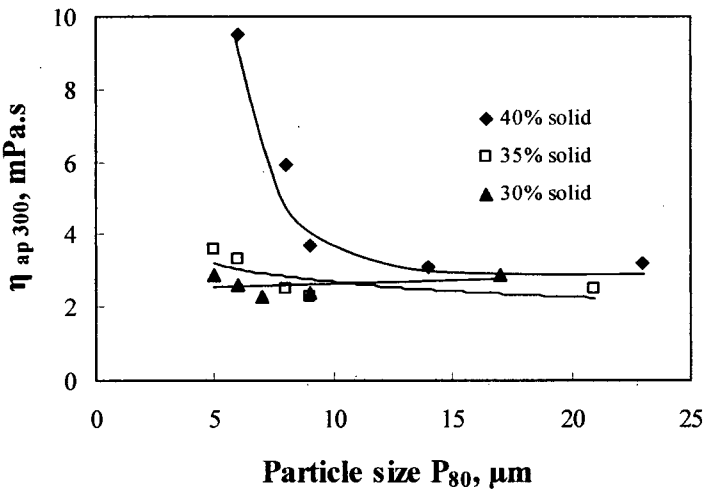

Figure 4.9 Apparent viscosity (300 s^{-1}) vs. particle size P_{80}

4.4.3 Breakage Rate

The specific breakage rate is commonly used as a parameter to describe breakage kinetics in comminution processes. The specific breakage rates were determined for the quartz slurries with solid contents of 30, 35 and 40% as shown in Figure 4.10.

Klimpel (1982, 1983) concluded that many coal and mineral slurries exhibit dilatant properties when the slurry density is less than 40-45% by weight. Above this range, the slurries became pseudo-plastic up to a solid content of about 75%. Below 75%, breakage rates were "first-order". Above 75% the slurries exhibited yield pseudo-plastic properties which corresponded with a significant decrease in breakage rate and a "non-first order" breakage relationship.

Unlike the results with tumbling mills, breakage rate in the stirred mill remained first- order despite the presence of a yield stress. The dilatant properties measured by Klimpel (1982, 1983) may be explained by particle settling during rheological measurements. For rod mill and ball mill pulps, the slurries would have settled very quickly at solid concentrations below 45%. With time, the sediment buildup at the bottom of the cup would impede the rotation of the bob and falsely produce results that appear to be dilatant.

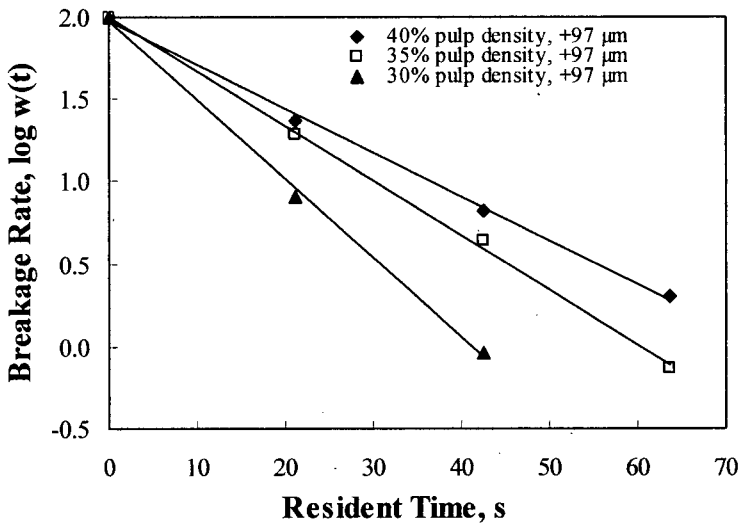

Figure 4.10 Specific breakage rate vs. pulp density with different top size fractions

In order to investigate the influence of yield stress on particle breakage rate, the specific breakage rate was plotted against slurry yield stress as shown in Figure 4.11. It is evident that slurry yield stress has a negative effect on particle breakage rate. An increased yield stress results in a slowing down in particle breakage rate for both 35% and 40% solids of slurries in the stirred mill. At 35% solids, the breakage rate is more sensitive to the variation in yield stress and slows down rapidly with a small increase in the yield stress till it reaches about 0.05 Pa. It was also observed that the initial specific breakage rate for 40% solids is lower than for 35% solids, indicating the strong influence of higher yield stress on particle breakage rate in the stirred mill.

Figure 4.12 shows the relationship between specific breakage rate and particle size. The comparison for the curves with 35% and 40% solids also show relatively high breakage rates at lower pulp density. The results suggest that below about 10 μm, the relationship between breakage rate and particle size is not linear. Previous results under similar grinding conditions suggested a linear relationship down to about 10 μm (Yue, Klein 2003).

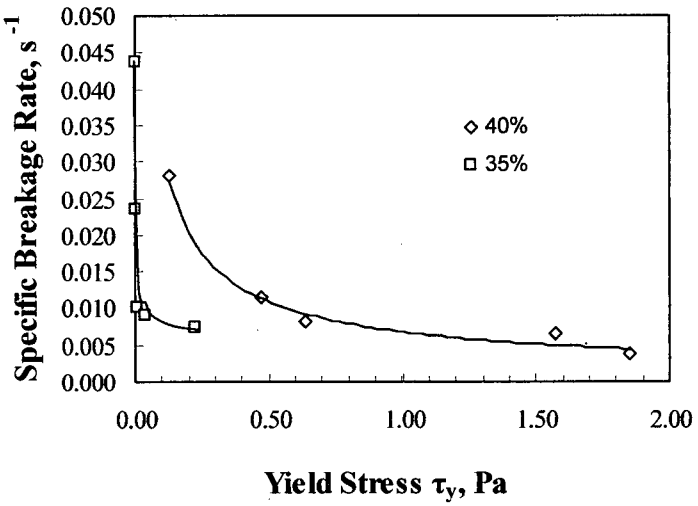

Figure 4.11 Specific breakage rate vs. pulp yield stress

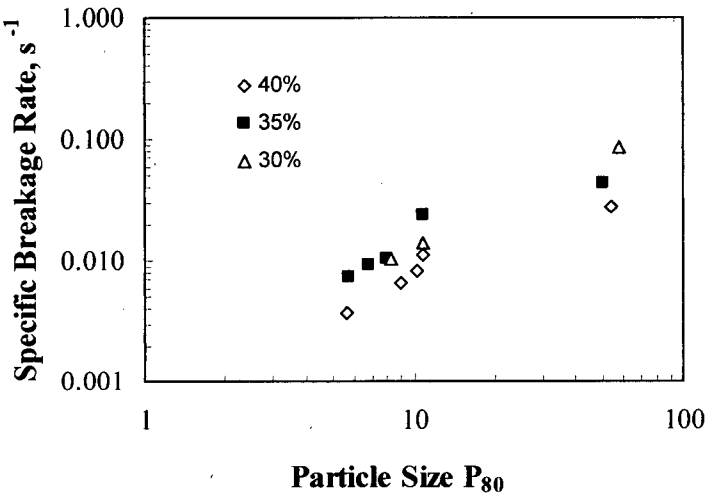

Figure 4.12 Specific breakage rate vs. particle sizes

The influence of the yield stress on breakage rates in stirred mills is demonstrated by comparing the rates at coarse and fine particles sizes. At coarser particle sizes (> 10 μm) the breakage rate decreased almost linearly up to 40% solids. Below this size (at 40% solids), the yield stress increased sharply (Figure 4.5) and the grinding rate decreased sharply (Figure 4.12). The results imply that the yield stress is responsible for decreased breakage rate.

4.4.4 Fines Production

Another indicator often used to evaluate grinding performance is fines production in the mill. Klimpel (1982, 1983) used the net production of material smaller than 75 μm as an index to evaluate the influence of rheology on ball mill grinding. Similarly the net production of fine -10μm material was used for this ultra-fine grinding study. Figure 4.13 shows the relationship between slurry yield stress and Net production of -10 μm at various feed sizes. Increasing yield

stress and decreasing feed size result in decreasing net production of -10 μm material. It seems that yield stress causes a slow down in the production of fines.

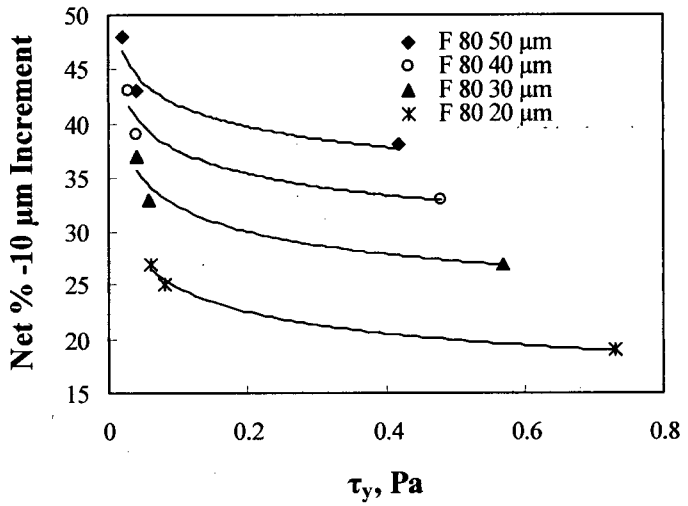

Figure 4.13 Net production of -10 μm vs. yield stress of slurries

4.4.5 Particle Size Distribution

In order to evaluate the influence of yield stress on grinding product size distribution, the Rosin-Rammler size distribution coefficient was plotted against slurry yield stress (Figure 4.14). The plot shows that as the yield stress increases, the distribution coefficient increases, indicating that size distribution becomes narrower. The effect of yield stress on size distribution is more significant at a lower solid content. At 35% solids, a small increase in yield stress from zero to about 0.4 Pa caused the distribution coefficient to increase from about 1.5 to 4.0. At 40% solids, the response was quite flat; changes in yield stress from 0.4 to 1.4 Pa caused the coefficient to change from about 1.0 to 1.5. The results demonstrate clearly the advantage of grinding at lower solid contents to create a narrower size distribution. As mentioned, this has potentially significant advantages with respect to down stream flotation and dewatering processes. These finding contradict those obtained by Kapur et al (1996) which indicated that comminuted

products are identical self similar curves and who concluded that the grinding mechanisms or rate cannot be altered.

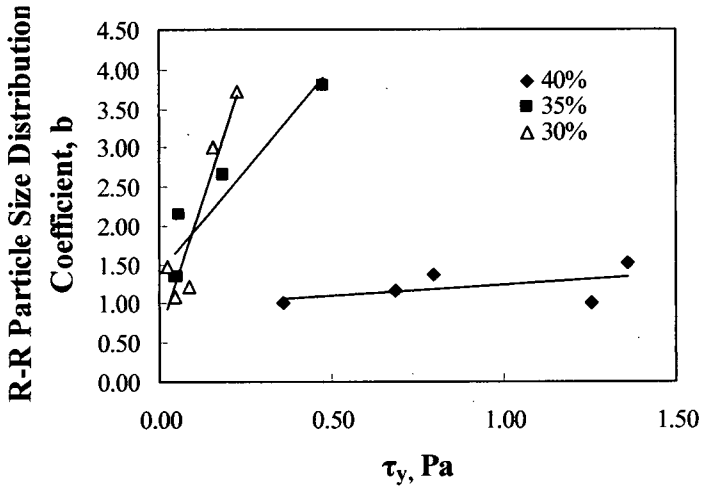

Figure 4.14 Rosin-Rammler particle size distribution coefficient vs. slurry yield stress

4.3.6 Power

Several papers have been published on stirred mill power prediction and optimization. Gao et al (1997) investigated the influence of various parameters on grinding power consumption for a pilot scale horizontal stirred bead mill. They reviewed the published information and found that most studies dealt only with the effect of stirrer speed on mill power. They developed an empirical model that related power to several parameters as show in Equation 4.4. They concluded that the dispersant dosage had small but significant linear effect on the mill power, indicating indirectly that rheological parameters affect mill power consumption.

$$P = 10^{9.29} (N)^{1.429} (\rho_s)^{2.90} (\rho_b)^{0.18} (d)^{-0.0.96} \qquad (4.4)$$

Where,

P is stirrer power, kW,

N is stirrer speed, rpm,

ρ_s is slurry solid content, %,

ρ_b is bead density, g/cc,

d is the dispersant dosage, %.

Gao and Forssberg (1993) suggested that stable operation in ultra-fine grinding depended on the slurry yield stress. When yield stress exceeded a limiting value, the mill shutdown due to power draw overload. As shown in Figure 4.15, the results of this study confirm that the yield stress strongly affects the grinding power. The figure shows that the mill power draw is proportional to slurry yield stress. With consideration of the effect of particle size on yield stress (Figure 4.5), it is evident that as particles become smaller the power draw will increase. The consequence is that a shaft power predicted using Equation 4 may vary with slurry rheological properties caused by feed size and size distribution.

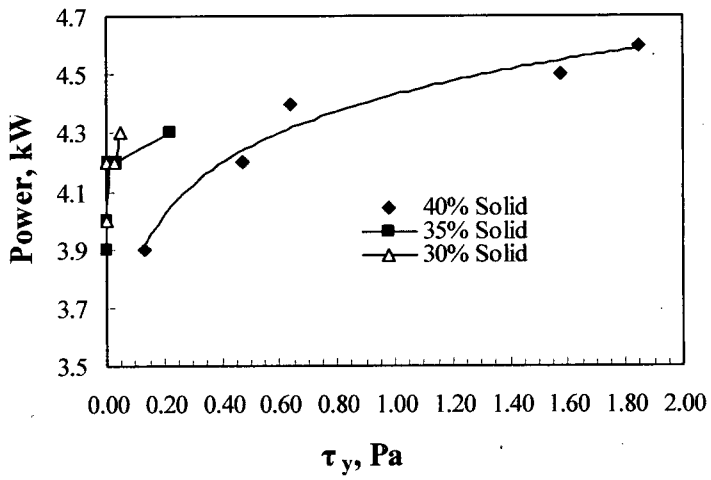

Figure 4.15 Agitator power vs. yield stress of slurries tested

The influence of slurry viscosity on mill power was also observed. Figure 4.16 is the plot of mill power draw against Casson viscosity. Unlike with the yield stress, there is no clear trend showing the relationship of the Casson viscosity on mill power draw. This result supports the conclusion that the Casson viscosity has a less important role in stirred mill grinding when compared to the yield stress.

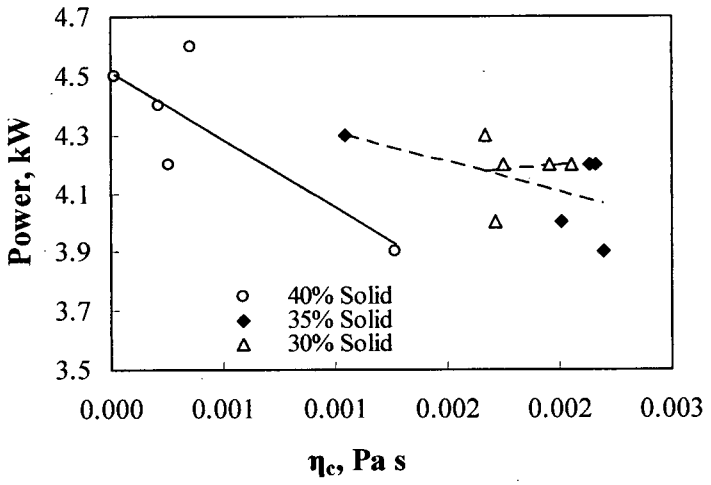

Figure 4.16 Agitator power vs. Casson viscosity of slurries tested

4.5 Conclusions

The rheological properties of quartz suspensions from the pilot scale horizontal stirred mill were determined and modeled using the Casson and Bingham equations. The results suggest that the suspensions are almost Newtonian at coarse particle sizes. As particle size decreases they become increasingly pseudo-plastic and eventually yield pseudo-plastic. Over the range of conditions studied in this research, dilatant properties were not observed. The Casson model fits better than the Bingham equation for the flow-curve data.

The slurry yield stress is affected by both solid content and particle size. The critical solid content is between 35 to 40% solids by weight, above which the yield stress increases exponentially. As particle sizes become smaller the critical solid content decreases. The yield stress is the dominant rheological parameter which influences ultra-fine grinding performance most.

The influence of slurry rheology on breakage kinetics was investigated. The research shows that contrary to other studies the yield pseudo-plastic behavior of quartz suspensions gives "first-order" breakage rate in stirred mills. The particle breakage rate is strongly affected by yield stress. At coarser particle size (P_{80}>10 μm) the breakage rate decreased almost linearly up to 40% solids. Below this size (at 40% solids) the yield stress increases sharply and the breakage rate decreased sharply. The results imply that the yield stress is responsible for decreased breakage rate.

The results demonstrate that below about 10 μm, the relationship between breakage rate and particle size is not linear. Previous results (Chapter 2) under similar grinding conditions demonstrated a linear relationship down to about 10 μm.

For fines production in the mill, it is demonstrated that increasing yield stress results in decreasing net production of -10 μm size fraction. Strong yield stress would slow down the production of fine particles and deteriorate milling performance.

Rosin-Rammler size distribution coefficient was applied to characterize the product size distributions. The results confirm that coefficient increases at lower yield stress, indicating that size distribution becomes narrower at a certain yield stress threshold. Over this limit, the size

distributions become wider. The yield stress impedes production of narrow size distribution, which may be important to down stream processes.

The power consumption of the stirred mill is sensitive to the variation of slurry yield stress. An increase in yield stress sharply increases the power consumption.

4.6 Recommendations

The research demonstrates slurry yield stress is the main rheological parameter that influences ultra-fine grinding in stirred mills. Therefore it is essential to investigate slurry yield stresses of minerals and industrial materials as much as possible at an industrial applicable range of solid content and particle size. A data base for predicting the slurry yield stresses at certain conditions can be created.

Ultimately the optimization of ultra-fine grinding can be accomplished through an industrial on line rheological monitor and control system.

Chapter 5 Effects of Bead Size on Ultra-Fine Grinding in a Stirred Mill

5.1 Introduction

The effects of grinding bead size and its composition on particle breakage rate, product size and size distribution, as well as mill power consumption in a stirred mill are investigated and evaluated. The objective of this study was to search for the appropriate bead size for stirred mills.

5.2 Literature Review

Stirred bead mills are used for ultra-fine grinding minerals and other materials to particle sizes below a few microns. The energy needed for breakage is transferred through the grinding media to the particles. For a given particle size, mineral type and specific energy input, the bead size plays a very important role in the comminution process, particularly with respect to the stress intensity and the stress number (Kwade 1999).

From a physical-mechanical point of view, two conditions need to be satisfied for breaking particles in a grinding mill: the grinding media must exert sufficient stress intensity to the particles and there must be direct contact between the media and the particles. For fine grinding, it has been recognized (Stehr et al 1987, Kwade 1999) that the specific energy consumption by stirred mills is less than that of tumbling mills. Due to the high media volumetric loading in stirred bead mills, the stress intensity and stress number per unit volume acting on particles is higher than in tumbling mills.

For brittle particles, massive fracture occurs when the overall stress acting on a particle exceeds a critical value resulting in particle disintegration and creating a large number of fragments. Attrition is associated with smaller stresses exerted on particle edges causing a continuous but slow loss of particle mass. It is understood that massive fracture of brittle solids results in a faster particle breakage rate than attrition.

Kwade (1999, 2002) assumed that the stress intensity (SI) is proportional to the kinetic energy of grinding media, and thus showed that it is proportional to both stirrer speed and bead size. The stress number (SN) is also proportional to stirrer speed as well as to the number of beads in the mill. Kwade (1999) presented the following expressions for SI and SN (Equations 5.1 and 5.2), which demonstrates these relationships.

$$SI \propto SI_{GM} = d^3_{GM}\, \rho_{GM} v_t^2 \qquad (5.1)$$

$$SN = N_C\, P_S / N_P \qquad (5.2)$$

Where:

GM is grinding media

d is the bead diameter

ρ is the bead density

v_t is the bead tangential velocity

N_C is the media contact number

P_S is the probability that a particle is caught and stressed by the media

N_P is the number of product particles inside the mill.

Blecher et al (1996) studied the motion of grinding media with disc stirrers. They showed that a high tangential velocity gradient exists near the surfaces of the discs and at the grinding chamber wall. At these areas, they suggested that the power intensity is much higher than the mean value for the mill and that more intensive collisions take place. These high intensity collisions are believed to account for most of the particle breakage in the mill.

The size of grinding balls is known to play a very important role in grinding in tumbling mills. In particular, small balls are important for effective compression and attrition of fine particles. Since the motion of mixture of beads, mineral particles and water in stirred mill chamber is at a very high speed, it is not clear if this is true for stirred mills.

So far the rheological concepts have been applied to the aqueous mineral suspension. These concepts may also be applied to the entire mixture within the mill as well. For aqueous mineral suspensions, the relative viscosity η_r increases with solid volume fraction Φ (Bicerano et al, 1999, Chong et al 1971) and increasing particle size d (Clark, 1968). Similarly, Wang and Forssberg (1997) observed that increasing bead volumetric loading (Φ) (bead mill) causes the power draw to increase greatly. Also, Herbst (1978) showed that increasing the bead size (d) increases the bead mill power draw. Both of these results demonstrate that the volume content and size of grinding media affect power in a similar manner to how particles affect rheology. It is apparent that changes in the physical properties of suspension that cause the viscosity to decrease correspond to changes in bead composition that lead to a reduction in power requirements. Therefore testing was carried out to demonstrate the effect of bead size on grinding in stirred mills, with respect to breakage kinetics, product size, size distribution and power consumption.

Research on the rheology of mineral suspensions has demonstrated that selected compositions of bimodal particle size distributions produce a "minimum" viscosity (Chong, 1971). This bimodal size distribution is also characterized by a maximum particle packing fraction. A study was conducted to assess the effect of bimodal bead size distribution on power usage, grinding rate and product size distribution.

5.3 Experiments

Experimental procedures are shown in Chapter 2 (test 8 to test 12).

5.4 Results and discussions

5.4.1 Mono-sized grinding beads

The ultra-fine grinding tests were conducted to evaluate the effects of bead size on particle breakage rate, product size, size distribution, as well as agitator power consumption. The bead size, agitator speed, and feed size were varied while the pulp density was kept constant during the tests.

Figure 5.1 shows how the specific breakage rate varies with bead size. At a constant agitator speed, the specific breakage rate increased almost linearly with bead size. When the mill power was kept constant, the specific breakage rate was highest at a bead size of 2 mm and the rates were lower when using smaller and larger beads. The "maximum" breakage rate at a bead size of

approximately 2 mm was observed for both feed materials (F_{80} 32 μm and F_{80} 83 μm). The significance of bead size was more pronounced for the coarser feed material.

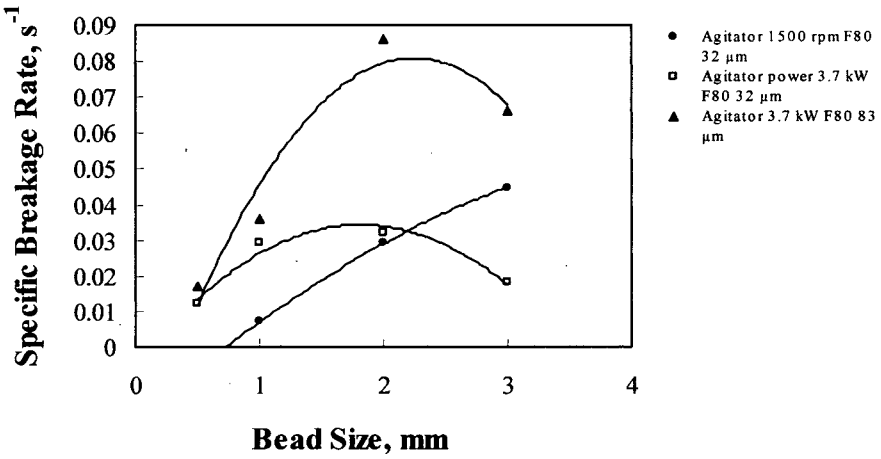

Figure 5.1 Specific breakage rate vs. bead size

When changing the bead size from 2 mm to 3 mm, the corresponding decrease in agitator speed at constant power draw had a greater impact on breakage rate than the increase in bead size. Using a smaller bead size caused a decrease in breakage rate implying a lower SI and a less effective use of power. There is insufficient information available to make conclusions to explain the reasons for the "optimum" bead size. Factors such as SI and SN likely play a role. However, the results of this study reveal that an optimum bead size can be selected. For example, the optimum may occur when the SN is maximum for bead of sufficient size to produce the SI needed to break particles.

Figure 5.2 shows how bead size affects product fineness (P_{80}). At constant agitator speed, increasing the bead size caused the product to become finer. However when grinding power was kept constant, there was an optimum bead size. For the 32 μm feed, the product size was finest when using a bead size of 1 mm. For the 83 μm feed, the 2 mm bead size produced the finest

product. In this case, when larger beads were used, the agitator speed had to be decreased to maintain a constant power. Conversely, when smaller beads were used, a higher agitator speed was required to maintain the same power.

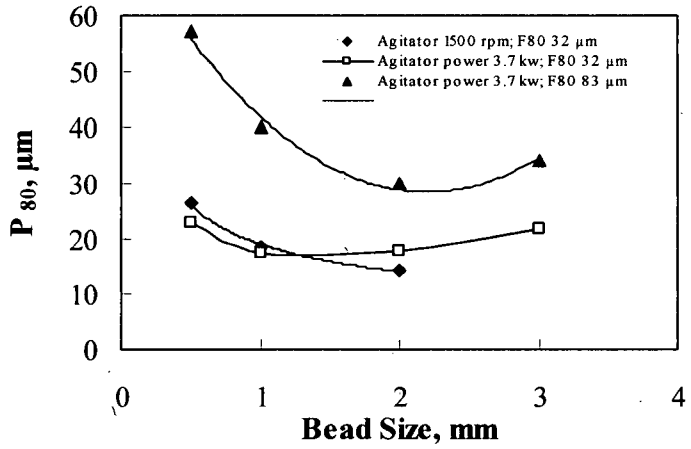

Figure 5.2 P_{80} vs. grinding bead size

The bead size also affects product size distributions (Figure 5.3). The product size distributions were characterized using the distribution coefficient from the fitted Rosin-Rammler equation. At constant power, larger beads produced a narrower size distribution. The results agreed with those obtained by Wang and Forssberg (2000). Since larger beads have higher kinetic energy, they have greater potential to cause massive fracture which produces a narrow product distribution. The smaller beads produce a wide size distribution, possibly due to the lower stress intensity promoting attrition over massive fracture.

For mineral processing, a narrower particle size distribution is usually preferred as it benefits downstream flotation and dewatering. If the goal is to produce a narrow product size distribution, the results presented in Figure 5.3 suggested that there is an optimum bead size.

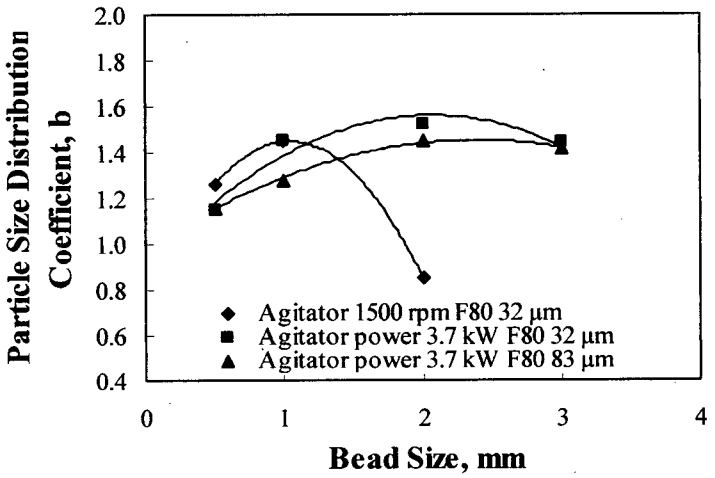

Figure 5.3 Particle size distribution coefficient vs. bead size

Figure 5.4 shows the relationship between bead size and agitator power draw (agitator speed was kept constant). Tests were performed with and without slurry to demonstrate the background effect of the grinding beads. Increasing the bead size causes the power draw to increase. In the presence of slurry, the power-draw increases more sharply than without slurry. Such relationship can also be interpreted by rheological concepts. Researchers (Chong, 1971, Clark, 1968) found that slurry viscosity increases with particle size. These results show that adding coarser beads increases the power draw, which implies an increased viscosity. The particles are filled into the bead voids and nipped, causing a strong shearing resistance that needs to be overcome by bead kinetic energy.

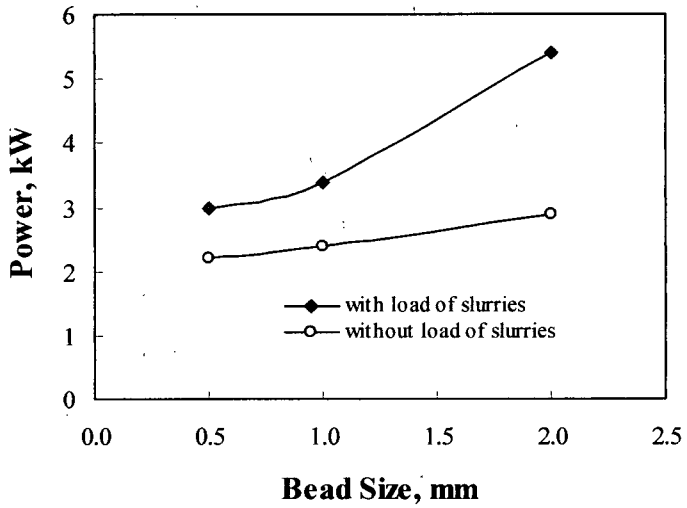

Figure 5.4 Agitator power vs. bead sizes

The results of the experiments showed that at constant agitator speed, increasing the bead size (to a limit):

- increases the breakage rate
- produced a finer product size
- generated a narrower product size distribution
- increased power usage

These results are supported by Equation 5.1 which shows that using larger beads will increase the stress intensity. These results demonstrate that factors that increase the stress intensity will increase grinding kinetics and produces a finer product. However, there is a trade-off as these factors also cause an increase in power usage.

In practice, mills are operated near the upper power limit. It is therefore important to understand how to "optimize" grinding at this constant upper power limit. The results reveal that at constant power draw, there was an optimum bead size with respect to a high breakage rate,

fineness of the product and narrow size distribution. The reasons for the optimum bead sizes cannot be readily explained by Equations 5.1 and 5.2.

Mankosa et al (1986) suggested that the optimum size ratio between beads and particles (mean size) is 20:1. Fadhel and Frances (2001) believed the ratio lies between 20:1 and 200:1. Figure 5.5 is a schematic diagram in which the ideal geometric dimensions of both beads and particles are assumed. Figure 5.5 a) shows there is one particle nipped by beads, in Figure 5.5 b) four to five particles are postulated captured in bead void for optimum breakage. The results calculated in Table 5.1 confirm that the "optimum" ratio between bead and particle is close to 20:1. The test data shown in Figures 5.1, 5.2 and 5.3 supports Mankosa's conclusion. In fact, the maximum breakage rate occurs when particles are large enough to have a high probability of contacting beads, but are small enough to be effectively caught and broken by the media. Above this limit, the breakage kinetics and size reduction ratio decrease. This decrease can be explained by geometric aspects of particle "nipping" or by a lower stress number SN (in Equation 5.2, P_S decreases and N_P increases simultaneously), although the stress intensity is kept constant.

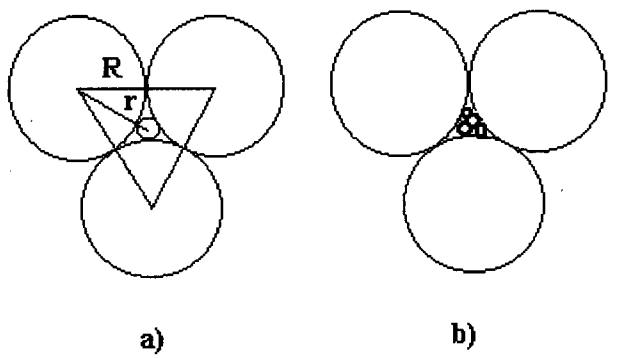

Figure 5.5 Schematic diagram of beads and particles in a stirred mill

Table 5.1 Relationship between bead diameter (D) and maximum particle size (*d*) based on geometries shown in Figure 6 where $d=2(R/\cos 30 - R)$.

D (mm)	3	2	1	0.5
a) *d* (mm)	0.46	0.3	0.15	0.076
b) *d* (mm)	0.15	0.1	0.05	0.025

Figure 5.6 presents the possible scenarios for impact and compression breakage in stirred bead mills. Schematic 5.6 a) shows collision between a particle and a bead. Schematic 5.6 b) shows particles captured in the void between beads are impacted indirectly by another bead. Schematic 5.6 c) illustrates particles being "roll-crushed" between beads. For case a), massive fracture occurs when the bead impacts the particle, but the probability of this impact is relatively low due to the great size difference between beads and particles. Case b) demonstrates the collision as balls hits the bed, in which impact energy is transferred through beads to particles indirectly, resulting in particle fracture. This is perhaps responsible for most of the particle breakage in stirred mills. The probability of case c) is also quite high. In this case, compression occurs between beads, which act as numerous tiny roll-crushers working in a mill. If particle sizes are too small, compression may be replaced by attrition.

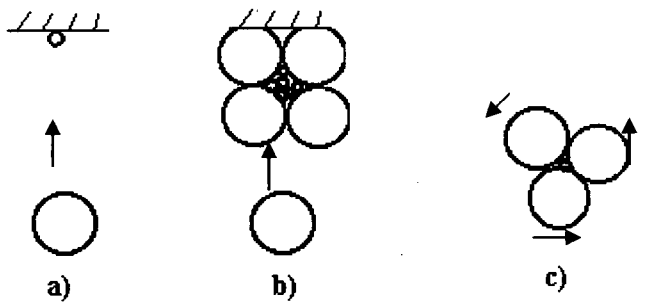

Figure 5.6 Schematic diagram of impact and compression breakage mechanism

5.4.2 Bead Size Distribution

There is the theoretical possibility of increasing charge mass load while keeping load volume constant by selecting the bead size distribution. In particular, the packing density of grinding media can be increased by filling the voids between the largest beads with smaller beads producing a bimodal bead size distribution. The maximum packing density for a bimodal distribution is achieved when ratio of particle sizes (small to large) is less than about 0.1 and when approximately 30% of the total volume is comprised of the smaller particles (Furnas, 1931). Chong (1971) found that the viscosity of suspensions at a fixed solid concentration was at a minimum when using this bimodal size distribution. The implication is that a bimodal bead size distribution would correspond to a minimum power draw.

For stirred mill grinding, the grinding media typically occupies about 80% of the mill volume. Introducing fine beads into a bed of coarse beads would theoretically increase the volume of solid fraction of beads by 24% from about 60% to about 84%. Therefore, adding small beads has the potential to increase the charge mass by 40% (24/60) while maintaining a constant charge volume. There would likely be a consequence of increasing the charge mass to grinding rate and power usage. However, there are practical limitations to maintaining such a bead size distribution during operation of an industrial mill.

In practice there is a distribution of bead sizes in grinding mills. During grinding the beads wear, reducing their size, and eventually pass through the mill product screen and rejected from the mill. There is a tradeoff between optimizing bead size with respect to grinding (size reduction, power usage, and product size distribution) and costs associated with media

consumption. It is therefore critical to determine the appropriate screen aperture to satisfy both of these criteria.

A set of experiments were conducted to assess the effect of changing the bead size distribution by increasing the proportion of fine beads. In particular, grinding tests were conducted using mixtures of 2 mm and 0.5 mm beads with compositions that varied from 100% coarse beads/0% fine beads to 0% coarse bead/100% fine beads. In order to maintain a constant charge volume for all experiments, the bulk densities of mixtures were determined (Figure 5.7). The graph shows that as the proportion of fine beads is increased, the bulk density increases; this result can be explained by the packing theory described above. However there is an unusual dip in the bulk density curve corresponding to fine fractions between 30% and 80%. It is suggested that this dip is a result of imperfect mixing which prevented optimum packing of the beads. Since optimum mixing would likely not be achieved in an operating mill, the measured bulk densities were used to prepare media compositions for the study.

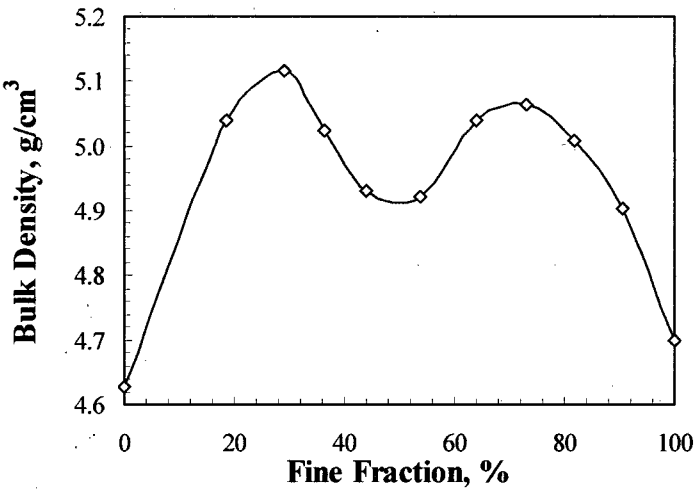

Figure 5.7 Bead bulk density vs. fine fraction of bi-modal beads

The experimental work was aimed at evaluating the effect of media wear. Tests were conducted using increasing proportions of fine media and determining the specific breakage rate, product particle size, size distribution and power consumption. The results are shown in Figures 5.8, 5.9, 5.10 and 5.11.

Under conditions of maintaining constant mill power or maintaining constant agitator speed, the specific breakage rate decreases as fine bead fraction increases (Figure 5.8). The decrease in breakage rate corresponds to an increase in product size (Figure 5.9). It is interesting to note that the product size distribution becomes wider by increasing the media fineness (Figure 5.10). The trend towards a wider size distribution and slower grinding rate can be interpreted as a change in grinding mechanisms from primarily massive fracture for the coarse media to attrition for the finer media. Figure 5.11 shows that the total power draw and net power draw decreased as the bead size became smaller.

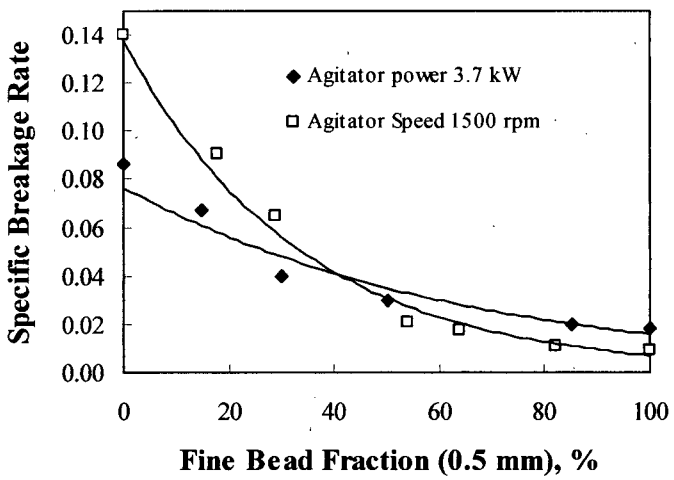

Figure 5.8 Specific breakage rate vs. % fine bead (F_{80} 83 μm)

If attrition is the main breakage mechanism, adding smaller beads, thereby increasing media surface area, should have caused the breakage rate to increase. Instead the breakage rate

decreased which implies that attrition is not the main breakage mechanism. This explanation supports the claim that massive fracture (impact) is the main breakage mechanism in horizontal stirred mills.

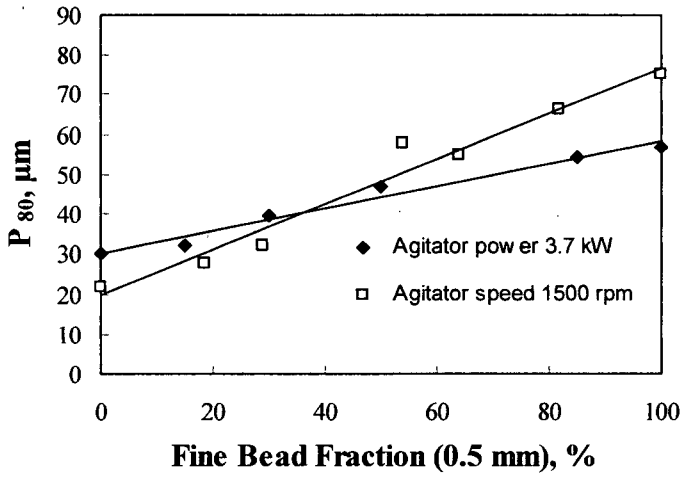

Figure 5.9 Product size P_{80} vs. grinding bead size (F_{80} 83 µm)

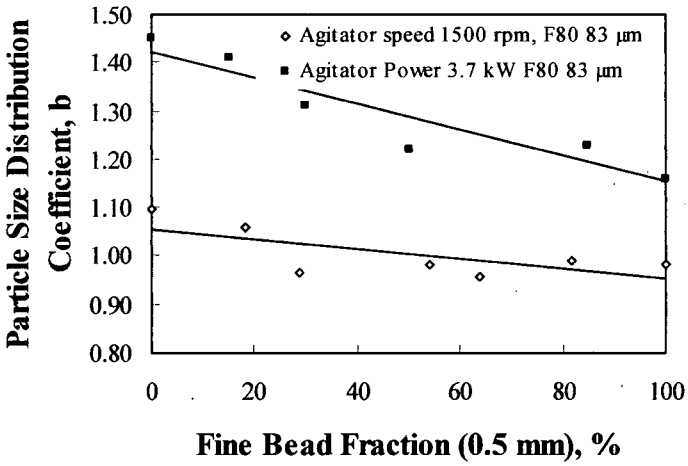

Figure 5.10 Particle distribution modulus vs. % fine bead

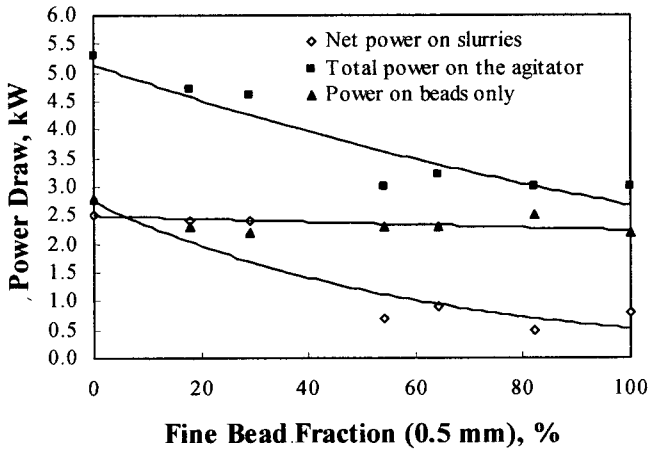

Figure 5.11 Agitator power vs. % fine bead.

Results from Figures 5.8, 5.9, and 5.10 show that the existence of fine beads affects milling performance greatly with respect to particle breakage rate, product size and size distribution even when the power input is kept constant. Figure 5.11 shows that replacing coarse beads with fine ones results in a decrease in power usage. The consequence of the build-up of fine media is that energy is not efficiently used and mills are not operated under "optimum" conditions.

All these results confirmed that fine beads in grinding media have negative effects in particle breakage rate, product size and size distribution, and are not in favor of grinding efficiency for stirred mills. The trends can be attributed to the lack of sufficient stress intensity in stirred mill when the beads become too fine.

In a ball mill used as secondary grinding for example, even small balls have sufficient energy to break particles through tumbling or rolling due to their relatively large diameter and heavy mass. However, it is the bead kinetic energy (high speed with a necessary mass) that breaks particles in stirred mills. Since the mass of fine bead is low, it may not exert sufficient

stress intensity on to particles at a certain circumferential speed. On the other hand, the mill power draw (bead viscosity) decreases due to the existence of small beads, as explained by "the ball bearing effects" theory (Chong et al 1971). This suggests that Chong's finding (1971) for bi-modal suspension applies to grinding beads in stirred mill. When beads move at a high speed, the fine beads behave as bearings and can alter the directions of coarser ones adjacent to them, thus buffer and lower the kinetic energy of coarse beads. The consequence is that the impact and compression force to break down particles with larger beads are weakened. These are believed to be the main breakage mechanisms in stirred mills.

5.5 Conclusions

Mono-sized and bimodal bead distributions were studied in a stirred bead mill for grinding quartz suspensions. The effects of bead size and its composition on particle breakage rate, product size and size distribution, as well as the mill power consumption are investigated and evaluated.

At a constant agitator speed for mono-sized grinding beads, increasing bead size increases mill power consumption resulting in a faster particle breakage rate, a finer product size, and a narrower size distribution. When the mill power draw is kept constant, there exist an optimum bead size for each feed size with respect to particle breakage rate, product size and size distribution. The optimum ratio of bead size to feed size is about 20:1.

Similar to suspensions, the viscosity of bimodal bead sizes (power consumption) is lower than viscosity of mono-sized beads. The fine beads in grinding media have lower stress intensity

and therefore have negative effects in particle breakage rate, product size and size distribution possibly due to "ball bearing effects", and are not in favor of grinding efficiency for stirred mills.

5.6 Recommendations

The massive fracture results in fast particle breakage and narrow particle size fraction in stirred mills. The bead kinetic energy contributes to the stress intensity and therefore the particle massive fracture as discussed in the study. It is essential to investigate bead motion theoretically both in water and in slurries by introducing a rheological parameter (yield stress for example) as to determine the loss of bead kinetic energy. A comparison of the difference in bead kinetic energy at certain rotating speeds in stirred mills can be determined and calculated in a similar way as Stoke's law for terminal velocity. Such a theoreticle study is both fundamental and practical to comminution process.

Chapter 6 Conclusions and Recommendations

6.1 Conclusions

Particle breakage kinetics, slurry rheological influences on breakage rate, product size and size distribution, as well as effects of bead sizes and its composition on ultra-fine grinding in a horizontal stirred mill are investigated.

The results of particle breakage kinetic studies confirm:

- The breakage rate is in "first-order" for tested slurries in the mill.
- The relationship of specific breakage rate and particle size for stirred mill is similar to those for tumbling mill.
- The population balance model can be applied to stirred mills.
- The breakage rate increases with decreasing solid content.
- The breakage rate decreases as the particle size becomes finer.
- Decreasing the solid content will produce a narrower size distribution.
- The product size distribution from stirred mill is better represented by the Rosin-Rammler equation than the Gaudin-Schuhmann equation.
- The Rosin-Rammler fit improves for products with a narrower size distribution and coarser particle size but is poor for particle sizes below three microns.
- The 10% top size fraction is most appropriate for the determination of specific breakage rates in a stirred mill.
- At a given set of grinding conditions the size reduction ratio decreases with the feed size and approaches 1.0, indicating that a grinding limit exists.

- The primary breakage mechanism in the horizontal stirred mills is massive fracture, near the grinding limit attrition becomes dominant.
- The practical grinding limit depends on the effective stresses created in the mill.
- The limit observed is likely a limitation of mill conditions rather than the material itself.

The results of rheological studies demonstrate:

- The suspensions are almost Newtonian at coarse particle sizes.
- As particle size decreases the slurries become increasingly pseudo-plastic and eventually yield pseudo-plastic.
- Over the range of conditions studied in this research, dilatant properties were not observed.
- The Casson model fits better than the Bingham equation for the flow-curve data.
- The slurry yield stress is affected by both solid content and particle size. The critical solid content is between 35 to 40% solids by weight, over which the yield stress increases exponentially.
- As particle sizes become smaller the critical solid content decreases.
- Yield stress is the dominant rheological parameter which influences ultra-fine grinding performance.
- The yield pseudo-plastic behavior of quartz suspensions give "first-order" breakage rate in stirred mills.
- The particle breakage rate is strongly affected by yield stress. At coarser particle size (>10 μm) the breakage rate decreased almost linearly up to 40% solids. Below about 10 μm, the relationship between breakage rate and particle size is not linear.

- Increasing yield stress results in decreasing net production of -10 μm size fraction.
- Rosin-Rammler size distribution coefficient increases at lower yield stress, indicating that size distribution becomes narrower at a certain yield stress threshold. Over this limit, the size distributions become wider.
- An increase in yield stress sharply increases the power consumption.

The results of bead size and size distribution tests suggest:

- At a constant agitator speed for mono-sized grinding beads, increasing bead size increases mill power consumption, results in fast particle breakage rate, fine product size, and narrow size distribution.
- When the mill power draw is kept constant, there exist optimum bead sizes for certain feed sizes with respect to particle breakage rate, product size and size distribution. The optimum ratio of bead size to feed size is confirmed about 20:1.
- Similar to suspensions, bimodal bead viscosity (power consumption) is lower than mono-sized beads.
- The existence of fine beads in coarse media have negative effects in particle breakage rate, product size and size distribution due to "ball bearing effects", and are not in favor of grinding efficiency for stirred mills.

6.2 Recommendations

The breakage kinetics was investigated and modeled using Austin's "first order" breakage model for a stirred mill. The study is only part of the modeling work. Further work needs to be done on the primary distribution function modeling for the products from stirred mills so that the

population mass balance model can be fitted and the characteristics (particle size and size distribution) of products from stirred mill can be predicted. Based on the results that demonstrate the ability to affect product size distribution, studies should be conducted to relate product size and size distribution to liberation.

It was confirmed that bimodal distributions of grinding products occur as particle sizes become smaller in the study. For optimization of ultra-fine grinding, it is necessary to investigate further on critical operating conditions for stirred mill, as a bimodal distribution of grinding product is not favored for down stream processes such as flotation and dewatering.

The research demonstrates slurry yield stress is the main rheological parameter that influences ultra-fine grinding in stirred mills. Therefore it is essential to investigate slurry yield stresses of minerals and industrial materials as much as possible at an industrial applicable range of solid content and particle size. A data base for predicting the slurry yield stresses at certain conditions can be created. Ultimately the optimization of ultra-fine grinding can be accomplished through an industrial on line rheological monitor and control system.

The massive fracture results in fast particle breakage and narrow particle size fraction in stirred mills. The bead kinetic energy contributes to the stress intensity and therefore the particle massive fracture as discussed in the study. It is essential to investigate bead motion theoretically both in water and in slurries by introducing a rheological parameter (yield stress for example) as to determine the loss of bead kinetic energy. A comparison of the difference in bead kinetic energy at certain rotating speeds in stirred mills can be determined and calculated in a similar way as Stoke's law of terminal velocity. Such a theoretical study is both fundamental and practical to comminution process.

Reference

Austin, L.G. 1990, Ball Mills, Semi-Autogenous Mills, and High Presure Grinding Rolls, The Pennsylvania State University, pp. 4.1-5.14.

Austin, L.G. Klimpel, R.R., Luckie, P.T. 1984, "The Process Engineering of Size Reduction", SME, Littleton, Colorado.

Austin, L.G. and Shah, I., 1983, "A method for interconversion of Mcrotrac and sieve size distributions", Powder Technology, 35, 271-278.

Bicerano, J. 1999, "Model for the viscosity of particle dispersions", J Macromol Sci Rev Macromol Chem Phys C39, 561-642.

Chong, J. S. et al 1971, "Rheology of concentrated suspensions", Journal of Applied Polymer Science, Vol 15, pp. 2007-2021.

Clarke, B. 1967, "Rheology of Coarse Settling Suspensions", Trans. Inst. Chem. Eng. 45, T251-256.

Cohen, H.E. 1983, "Energy Usage in Mineral Processing", Trans Inst Min Metal, 92, C160-C163.

Enderle, U et al 1997, "Stirred mill technology for regrinding McArthur River and Mount Isa zinc/lead ores", Proceeding of the XX IMPC Aachen, pp. 71-78.

Epstein, B. 1947, "The material description of certain breakage mechanisms leading to the logarithmic –normal distribution", Franklin Inst., 244-471.

Furnas, C.C. 1929, "Flow of Gases through Beds of Broken Solid", Bureau of Mines, Bulletin 307, pp. 75-79.

Furnas, C. C. 1931, "Grading Aggregates", Industrial and Engineering Chemistry, Vol. 23, No 9, pp. 1052-1064.

Gau, M., Forssberg, E. 1993, "The Influence of slurry rheology on ultra-fine grinding in a stirred ball mill," XVIII IMPC, Sydney, Vol. 1, pp 237-244.

Gao, M.W., Forssberg, K.S.E., Weller, K.R. 1996 "Power Predictions for a Pilot Scale Stirred Ball Mill", Int. J. Miner. Process, Vol 44/45, pp641-652.

Herbst, J. A. 1978, "Fundamentals of fine and ultrafine grinding in a stirred ball mill", International Powder and Bulk Solids Handling Conference, Chicago. IL, pp.452-470.

Herbst, J. A. and Fuerstenau, D. W. 1968, "The zero order production of fines in comminution and its implication in simulation", Trans. SME/AIME 241, pp 531-549.

Herbst, J. A. and Fuerstenau, D. W. 1973, "Mathematical simulation of dry ball milling using specific power information", Trans. SME/AIME, pp 254-348.

Hogg, R., 1999, "Breakage mechanisms and mill performance in ultrafine grinding", Powder Technology 105, pp. 135-140.

Kapur, P. C., et al. 1996, "Role of dispersants in kinetics and energetics of stirred ball mill grinding"' Int. J. Miner. Process. 47, pp. 141-152.

Klein, B., Laskowski, J.S. and Partridge, S.J. 1995 "A New Viscometer for Rheological Measurements on Settling Suspensions," J. of Rheology, 39(5), pp. 827-840.

Klimpel, R.R. 1988, "Grinding Aids Based on Slurry Rheology Control," Reagents in Mineral Technology, Ed. P. Somasundaran, B. Moudgil, Marcel Dekker, NY, pp. 179-194.

Klimpel, R.R. 1982,1983, "Slurry Rheology Influence on the Performance of Mineral/Coal Grinding Circuits", Min. Eng., 34, pp 1665-1668, 35, pp 21-26.

Klimpel, R.R. 1998 " The Impact on Industrial Grinding Circuits of Changing and/or Controlling the Slurry Rheology", Comminution Practices, Ed. S.K. Kawatra, SME, Littleton Colorado, pp 1-9.

Kwade, Arno 1999, "Wet comminution in stirred media mills-research and its practical application", Powder Technology 105, pp. 14-20.

Kwade, Arno and Schwedes, Joerg 2002, "Breaking characteristics of different materials and their effect on stress intensity and stress number in stirred media mills", Powder Technology 122, pp. 109-121.

Liddel, K.S., Hall, S.J. 1999, "Stirred Vertical Mills for Ultra Fine Grinding", ANI-Metprotech.

Mankosa, J. 1986, "effect of media size in stirred ball mill grinding of coal", Powder Technology 49, pp. 75-82.

Napier-Munn, T.J., Shi, F. and Asomah, I.K. 1996, "Rheological Effects in Grinding and Classification", Min. Pro. Met. Rev., Vol. 20, pp 123-131.

Rosin, P and Rammler, E 1933/34, "The laws governing the fineness of powered coal", J Inst. Fuel, 7, (29).

Schuhmann, R 1940, "Principles of comminution, 1- size distribution and surface calculation", Tech Pubs AIME, No. 1189, 11.

Shinohara, Kunio 1999, "Fine grinding characteristics of hard materials by attrition mill", Powder Technology 103, pp. 292-296.

Stehr et al 1987, "Comparison of energy requirement for conventional and stirred ball milling of coal-water slurries", Coal Prep., Vol. 4, pp. 209-226.

Tromans, D. and Meech, J. D. 2002, "Fracture toughness and surface energies of minerals: theoretical estimates for oxides, sulphides, silicates and halites", Minerals Engineering, 15, 1027-1041.

Tuunila, R., Nystrom, L. 1997, "Wet Fine Grinding with the Attrition Bead Mill - Optimisation and Modelling of Grinding", Proc. Of the XX IMPC, Aachen Germany, pp 327-336.

Velamakani, V and Fuerstenau, W. D. 1993, "The effect of the adsorption of polymeric additives on the wet grinding materials—2. Dispersion and fine grinding of concentrated suspensions", Powder Technology 75, pp. 11-19.

Wang, Y., and Forssberg, E. 1997, "Ultra-Fine Grinding and Classification of Minerals", Comminution Practices, Ed. S.K. Kawatra, SME, Littleton Colorado, pp. 203-214.

Whiten, W.J., 1974, "A matrix theory of comminution machines", Chem. Eng. Sci. 29, pp 588-599.

Williams, E. J. (Evan James) "Regression analysis", New York, Wiley 1959, A Wiley publication in applied statistics.

Yan, D.S., Dunne, R.C., Freeman, M.E. 1995, "Efficiency of Stirred Ball Mills", Proc. XIX Int. Min. Proc. Congr., Littleton, Colorado, pp. 83-87.

Yue, J, and Klein, B. 2003, "Particle Breakage Kinetics in Horizontal Stirred Mills", CIM AGM 2003, Montréal.

Appendix A Grinding Kinetics and Rheology

A.1 Operating Conditions and Responses

The operating conditions and responses are shown in Table A.1.

Table A.1 Operating conditions and responses

Test No	Pulp Density	Agitator Speed	Pump Flow Rate	Pressure	Temperature	Power Draw
	% Solids	rpm	L/Min.	Pa	^{0}C	kW
1	35	1500	3.10	0.2	44	5.3
2.1	40	1500	1.68	0.2	52	3.9
2.2	40	1500	1.68	0.2-0.4	52	4.2
2.3	40	1500	1.68	0.2-0.4	49	4.4
2.4	40	1500	1.68	0.2-0.4	58	4.5
2.5	40	1500	1.68	0.4	50	4.6
3.1	35	1500	1.68	0.2	47	3.9
3.2	35	1500	1.68	0.2	52	4.0
3.3	35	1500	1.68	0.2	48	4.2
3.4	35	1500	1.68	0.2-0.4	50	4.2
3.5	35	1500	1.68	0.4	48	4.3
4.1	30	1500	1.68	0.2	45	4.0
4.2	30	1500	1.68	0.2	53	4.2
4.3	30	1500	1.68	0.2	52	4.2
4.4	30	1500	1.68	0.2	56	4.2
4.5	30	1500	1.68	0.2	55	4.3
5.1	40	1500	3.10	0.2	33	3.3
5.2	40	1500	3.10	0.2	34	3.3
5.3	40	1500	3.10	0.2	34	3.3
6.1	35	1500	3.10	0.2	33	3.3
6.2	35	1500	3.10	0.2	34	3.3
6.3	35	1500	3.10	0.2	34	3.3
7.1	30	1500	3.10	0.2	33	3.3
7.2	30	1500	3.10	0.2	33	3.3
7.3	30	1500	3.10	0.2	33	3.3

A.2 Particle Size Distributions

The particle size distribution curves of the grinding products are shown in Figure A.2.1, 2.2, 2.3, 2.4, and 2.5.

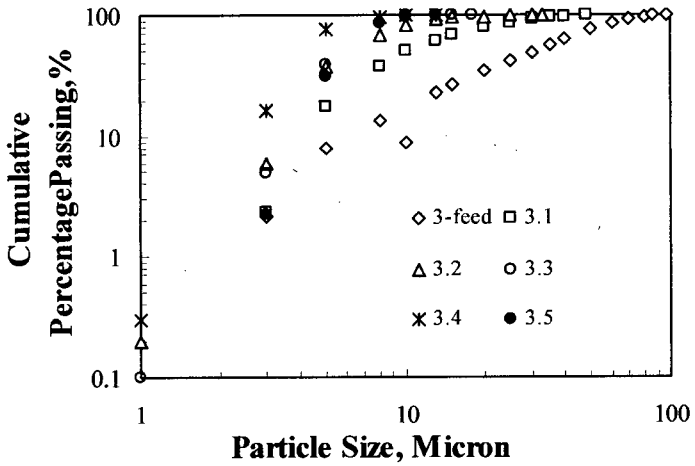

Figure A.2.1. Particle size distributions for test series 3 (35% solids)

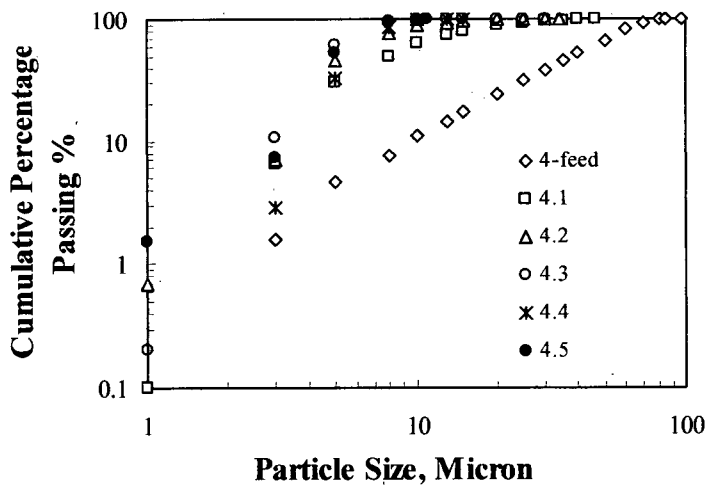

Figure A.2.2. Particle size distributions for test series 4 (30% solids)

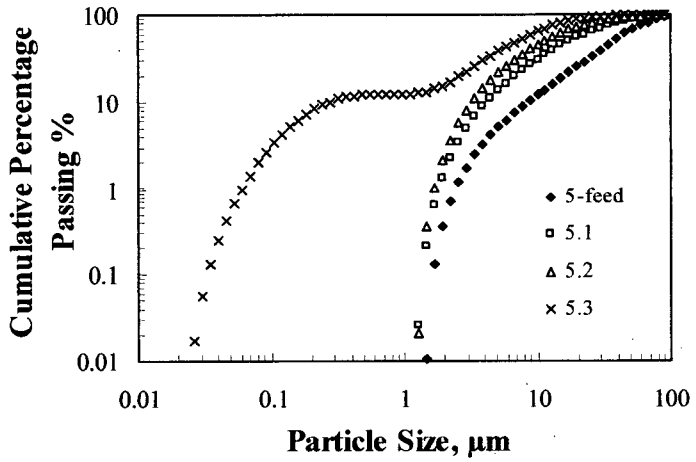

Figure A.2.3. Particle size distributions for test series 5 (40% solids)

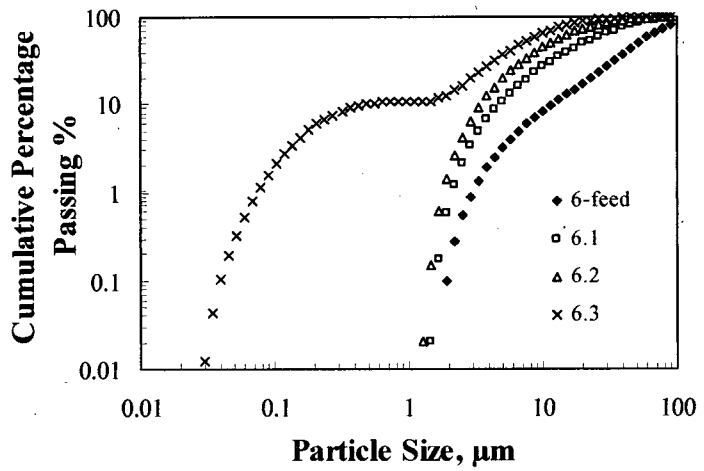

Figure A.2.4. Particle size distributions for test series 6 (35% solids)

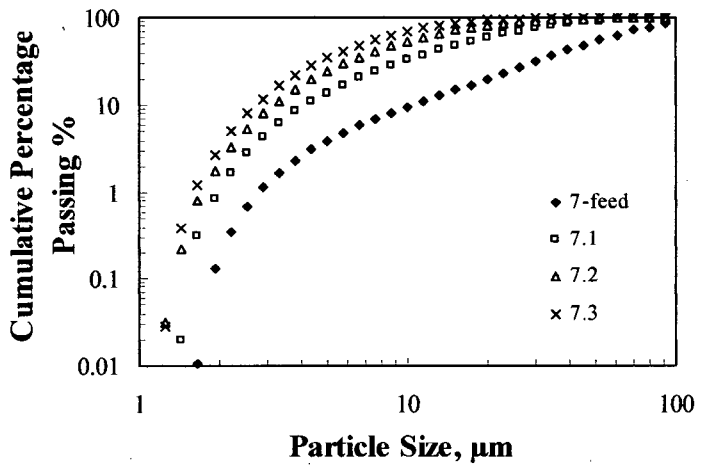

Figure A.2.5. Particle size distributions for test series 7 (30% solids)

A.3. PSD comparison

PSD result difference for a same slurry sample using the Malvern and Elzone particle size analyzers is shown in Figure A.3.1.

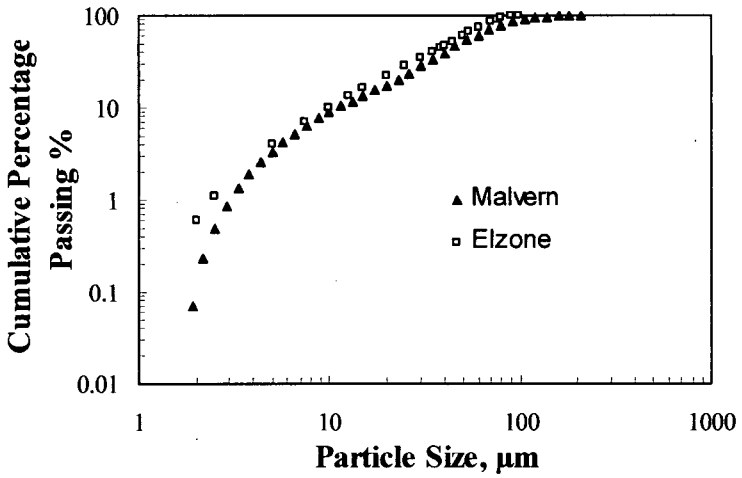

Figure A.3.1. PSD results for the Malvern and Elzone

A.4 Flow-Curves of Grinding Products

The particle size distribution curves of the grinding tests are shown in Figure A.4.1, 4.2.

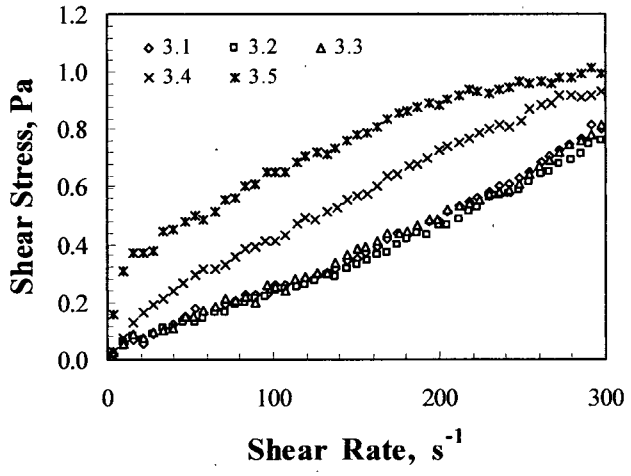

Figure A.4.1 Flow-curves of grinding products (35% solids)

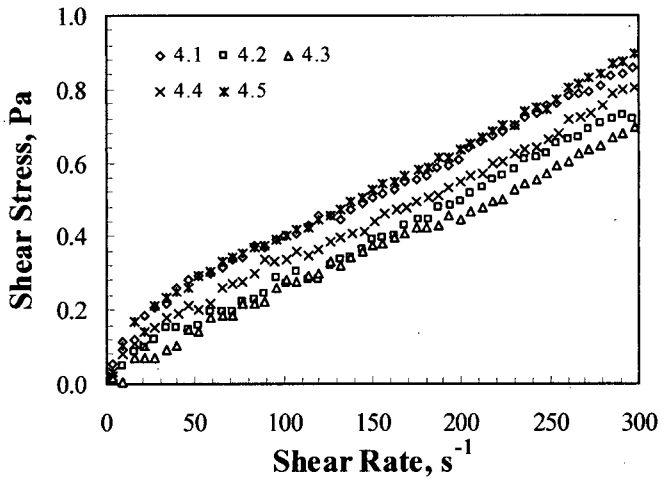

Figure A.4.2 Flow-curves of grinding products (30% solids)

A.5 Correlation Coefficient for the Casson and Bingham Equations' Fit

The correlation coefficient for the Casson and Bingham equations fit is shown in Figure A.5.1.

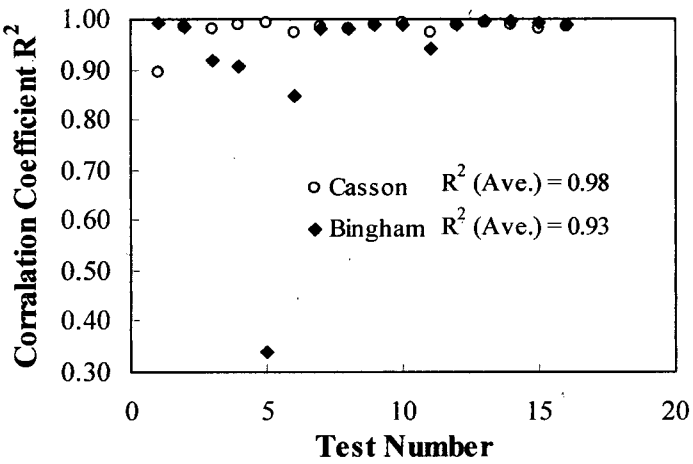

Figure A.5.1 Correlation coefficient vs. test number

A.6. Parameter Calculations

The parameters obtained from calculation and model fitting are listed in Table A.6.1, A.6.2 and A.6.3.

Table A.6.1. Specific breakage rate

Test No	Top Size	Pulp Density	Top Size Fraction with Time t		Resident Time t	Specific Breakage Rate
	µm	% solids	Absolute %	Relative %	s	S_i
5.F	+ 97	40	10.00	100.0	0	0.027
5.1			2.35	23.5	21.2	
5.2			0.67	6.7	42.4	
5.3			0.20	2.0	63.6	
6.F		35	14.30	100.0	0	0.033
6.1			2.86	19.1	21.2	
6.2			0.65	4.3	42.4	
6.3			0.11	0.7	63.6	
7.F		30	11.00	100.0	0	0.048
7.1			0.90	8.2	21.2	
7.2			0.10	0.9	42.4	
5.1	+ 64	40	9.60	100.0	0	0.024
5.2			3.41	34.1	21.2	
5.3			0.96	9.6	42.4	
6.1		35	10.51	100.0	0	0.032
6.2			2.96	19.7	21.2	
6.3			0.64	4.3	42.4	
7.1		30	5.25	100.0	0	0.038
7.2			1.02	9.3	21.2	
7.3			0.26	2.4	42.4	

Table A.6.2 Summary of Rheological Test Results

Test No	Yield Stress, τ_{yC}	Casson Viscosity, η_C	Apparent Viscosity, η_{ap} 50	Apparent Viscosity, η_{ap} 300	Yield Stress, τ_{yB}	Bingham Viscosity, η_B	Corealation Coefficient R^2	
	Pa	m. Pa	m. Pa	m. Pa	Pa	m. Pa	Casson	Bingham
2.F	0.010	2.60	4.20	3.20	0.06	3.0	0.90	0.99
2.1	0.132	1.27	7.60	3.20	0.24	2.5	0.99	0.99
2.2	0.472	0.26	12.90	3.10	0.55	1.4	0.98	0.92
2.3	0.637	0.21	16.20	3.70	0.72	1.4	0.99	0.91
2.4	1.573	0.02	33.10	5.90	1.57	0.8	0.99	0.34
2.5	1.846	0.36	44.60	9.50	2.04	2.9	0.97	0.85
3.F								
3.1	0.002	2.20	2.90	2.50	0.00	2.6	0.99	0.98
3.2	0.003	2.01	2.70	2.30	0.00	2.4	0.98	0.98
3.3	0.004	2.13	3.00	2.50	0.01	2.5	0.99	0.99
3.4	0.035	2.16	5.30	3.30	0.12	2.9	0.99	0.99
3.5	0.225	1.04	9.90	3.60	0.37	2.4	0.97	0.94
4.F								
4.1	0.000	1.71	5.10	2.90	0.14	2.5	0.99	0.99
4.2	0.008	1.95	3.20	2.40	0.04	2.4	0.99	0.99
4.3	0.002	2.05	2.70	2.30	0.03	2.2	0.99	0.99
4.4	0.025	1.75	4.10	2.60	0.08	2.4	0.98	0.99
4.5	0.052	1.67	5.30	2.90	0.13	2.6	0.99	0.99
5.F								
5.1	0.029	2.20	5.00	3.20	0.09	3.0		
5.2	0.067	1.81	6.30	3.30	0.17	2.8		
5.3	0.007	2.23	3.50	2.70	0.06	2.5		
6.F								
6.1								
6.2	0.003	2.32	3.10	2.60	0.00	2.7		
6.3	0.030	1.93	4.70	2.90	0.11	2.6		
7.F								
7.1	0.032	1.84	4.70	2.80	0.10	2.6		
7.2	0.005	2.00	3.00	2.40	0.03	2.4		
7.3	0.099	1.29	6.50	2.90	0.19	2.4		

Table A.6.3 Summary of Particle Size Test Results

Test No	Particle size P_{80}	-10µm Fraction	R-R Dist. Coefficient	R-R Size Coefficient	Correlation coefficient R^2	
	µm	%	b	a	Gaudin-Schuhmann	Rosin-Rammler
2.F	66	10	1.57	45.5	0.96	0.98
2.1	23	52	1.00	13.7	0.82	0.99
2.2	14	71	1.16	9.1	0.70	0.99
2.3	9	84	1.37	7.4	0.79	0.89
2.4	8	92	1.02	3.9	0.75	0.88
2.5	6	97	1.51	5.8	0.84	0.99
3.F	58	9	1.35	35.1	0.94	0.98
3.1	21	52	1.34	14.5	0.79	0.98
3.2	9	84	1.34	7.4	0.81	0.97
3.3	8	97	2.15	6.4	0.90	0.95
3.4	6	99	2.66	5.2	0.89	0.95
3.5	5	100	3.77	6.5	0.86	0.99
4.F	59	11	1.46	45.3	0.98	0.99
4.1	17	63	1.46	12.2	0.77	0.95
4.2	9	88	1.22	6.2	0.81	0.97
4.3	7	97	1.08	3.7	0.76	0.87
4.4	6	99	3.02	6.5	0.82	0.96
4.5	5	100	3.17	5.8	0.96	0.99
5.F	75	10	1.38	53.9	0.98	0.99
5.1	44	26	1.27	29.8	0.91	0.98
5.2	28	41	1.21	20.8	0.85	0.97
5.3	17	59	0.80	10.9	0.92	0.95
6.F	90	8	1.38	64.8	0.98	0.99
6.1	46	27	1.25	30.6	0.90	0.98
6.2	25	45	1.24	19.6	0.82	0.95
6.3	15	65	0.87	10.1	0.92	0.96
7.F	81	10	1.36	58.2	0.98	0.99
7.1	35	33	1.27	24.5	0.89	0.98
7.2	19	53	1.30	15.6	0.82	0.96
7.3	13	69	1.26	11.3	0.75	0.94

Appendix B Bead Size Testing

B.1 Particle Size Distributions

The particle size distribution curves of the grinding products are shown in Figure B.1.1, 1.2, 1.3, 1.4, and 1.5.

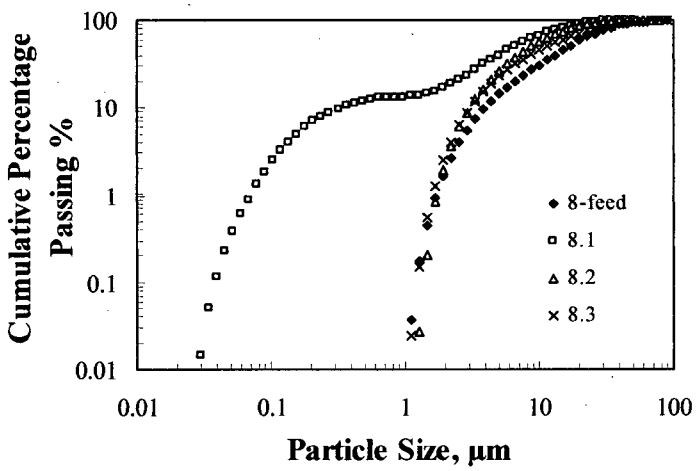

Figure B.1.1. Particle size distributions for test series 8 (35% solids)

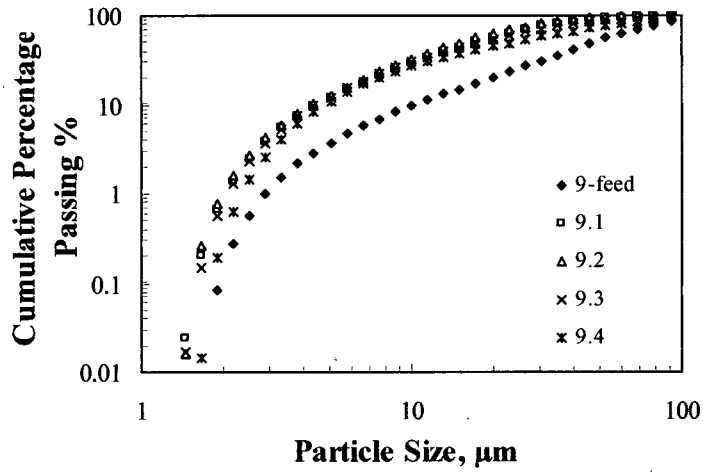

Figure B.1.2. Particle size distributions for test series 9 (35% solids)

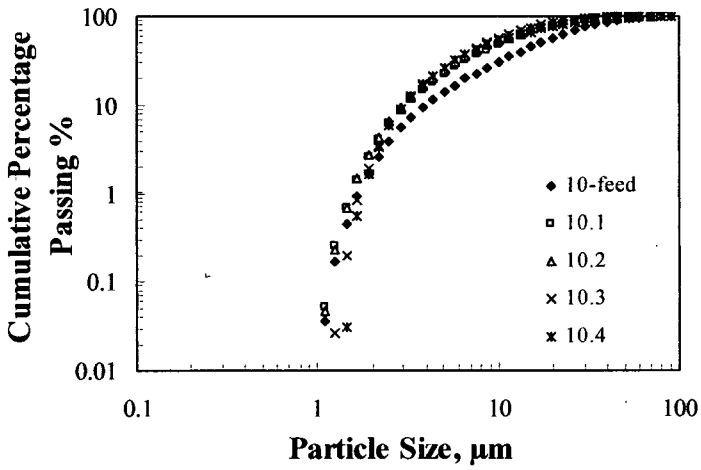

Figure B.1.3. Particle size distributions for test series 10 (35% solids)

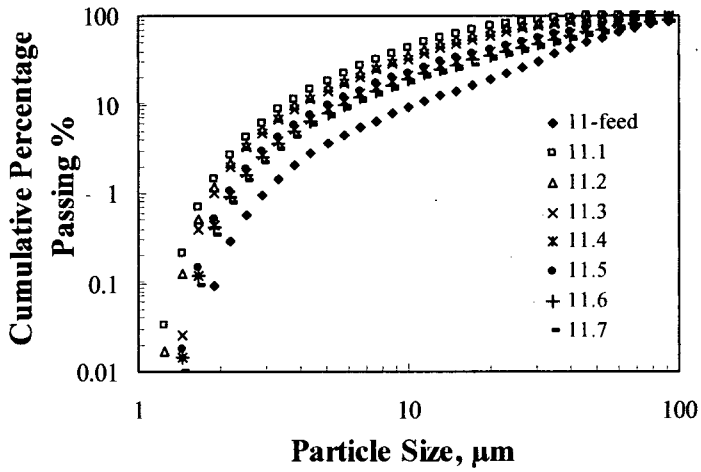

Figure B.1.4. Particle size distributions for test series 11 (35% solids)

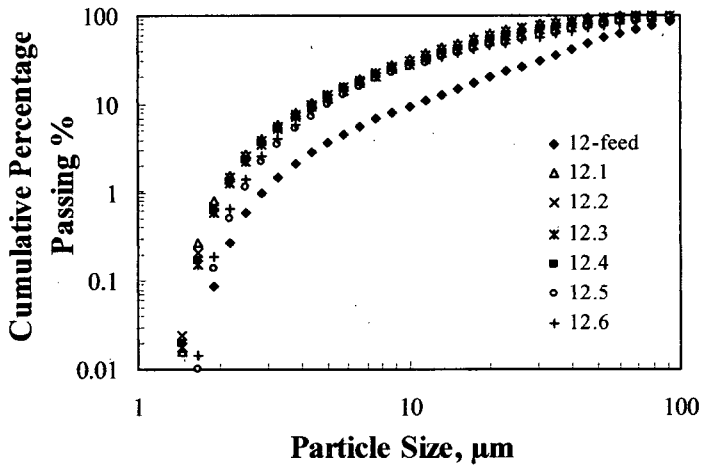

Figure B1.5. Particle size distributions for test series 12 (35% solids)

B.2 Determination of Bimodal Bead Composition

The data for bimodal bead composition are listed in Table B.2.1.

Table B.2.1 Bimodal bead composition test D 2mm, *d* 0.5mm, Total volume 1000ml

Bulk Vol. ml		Weight	Voids	Absolute Bead Vol. ml		Bulk Density	
D	*d*	g	ml	D	*d*	% Vol. of *d*	g/cm^3
1000	0	4736.2	364	636.0	0	0	4.74
900	130	4853.5		572.4	84.4	13	4.85
800	250	4963.5		508.8	162.3	24	4.96
700	362	5025.4		445.2	234.9	35	5.03
600	445	4975.4		381.6	288.8	43	4.98
500	530	4909.8		318.0	344.0	52	4.91
400	612	4889.1		254.4	397.2	61	4.89
300	750	5007.6		190.8	486.8	72	5.01
200	822	4982.4		127.2	533.5	81	4.98
100	912	4883.0		63.6	591.9	90	4.88
0	1000	4788.2	351	0	649.0	100	4.79

B.3 Operating Conditions and Parameter calculations

The operating conditions and parameter calculations are listed in Table B.3.1.

Table B.3.1 Operating conditions and calculation

Test No	Bead	Fine Bead	A. Speed	Power	S.B. Rate	R-R Dist.	Prod. Size	Correlation coefficient R^2	
	mm	%	rpm	kW	S_i	b	P_{80}	G-S	R-R
8.1	2	—	1500	5.6	0.045	0.85	14.2	0.92	0.95
8.2	1	—	1500	3.7	0.029	1.45	17.4	0.86	0.97
8.3	0.5	—	1500	2.7	0.007	1.26	26.2	0.99	0.96
9.1	3	—	1160	3.7	0.066	1.42	34.0	0.90	0.97
9.2	2	—	1310	3.7	0.086	1.45	30.1	0.89	0.97
9.3	1	—	1500	3.7	0.036	1.28	40.2	0.86	0.97
9.4	0.5	—	1650	3.7	0.017	1.16	57.1	0.84	0.96
10.1	3	—	1160	3.7	0.018	1.44	21.6	0.93	0.98
10.2	2	—	1320	3.7	0.032	1.52	17.8	0.93	0.99
10.3	1	—	1500	3.7	0.029	1.45	17.4	0.90	0.97
10.4	0.5	—	1700	3.7	0.012	1.15	22.6	0.89	0.97
11.1	(2 + 0.5)	0	1500	5.4	0.14	1.10	22.0	0.90	0.98
11.2	(2 + 0.5)	18	1500	4.7	0.09	1.06	27.5	0.91	0.98
11.3	(2 + 0.5)	29	1500	4.6	0.07	0.97	31.9	0.92	0.99
11.4	(2 + 0.5)	54	1500	3.1	0.02	0.98	58.0	0.93	0.98
11.5	(2 + 0.5)	64	1500	3.2	0.02	0.96	55.0	0.92	0.98
11.6	(2 + 0.5)	82	1500	3.0	0.01	0.99	66.3	0.94	0.98
11.7	(2 + 0.5)	100	1500	3.0	0.01	0.98	75.0	0.94	0.98
12.1	(2 + 0.5)	0	1310	3.7	0.09	1.45	30.0	0.93	0.99
12.2	(2 + 0.5)	15	1440	3.7	0.07	1.41	32.3	0.92	0.99
12.3	(2 + 0.5)	30	1570	3.7	0.04	1.31	39.5	0.91	0.98
12.4	(2 + 0.5)	50	1640	3.7	0.03	1.22	47.0	0.90	0.98
12.5	(2 + 0.5)	85	1645	3.7	0.02	1.23	54.2	0.90	0.97
12.6	(2 + 0.5)	100	1650	3.7	0.02	1.16	57.0	0.89	0.97